Aerospace Science and Technology 32 (2014) 66–83

Contents lists available at ScienceDirect

Aerospace Science and Technology

www.elsevier.com/locate/aescte

Elastic/plastic buckling of isotropic thin plates subjected to uniform and linearly varying in-plane loading using incremental and deformation theories

M. Kadkhodayan *, M. Maarefdoust

Department of Mechanical Engineering, Ferdowsi University of Mashhad, Mashhad 91775-1111, Iran

ARTICLE INFO

Article history:
Received 16 July 2013
Received in revised form 8 November 2013
Accepted 7 December 2013
Available online 12 December 2013

Keywords:
Thin plate
GDQ method
Elastic/plastic buckling
Linearly varying loading

ABSTRACT

The present study is concerned with the elastic/plastic buckling of thin rectangular plates under various loads and boundary conditions. The in-plane loads are placed uniformly and linearly varying in the uniaxial compression and biaxial compression/tension. The equilibrium and stability equations are derived and analyses are carried out based on two theories of plasticity, i.e. deformation theory (DT) and incremental theory (IT). The elastic/plastic behavior of plates is described by the Ramberg–Osgood model. Generalized Differential Quadrature (GDQ) discretization technique is used to solve the buckling of plate equation. To examine accuracy of the present formulation and procedure, several convergence and comparison studies are investigated and new results are presented. The differences between the IT and DT results increase by increasing loading parameter in linearly varying in-plane loading. Some new consequences are achieved regarding the validation range of two theories. Furthermore, effects of aspect, thickness to length and loading ratios, boundary condition, type of plasticity theory and linearly varying in-plane loading on the buckling coefficient are discussed. Contour plots of buckling mode shapes for various loading parameters are also illustrated.

1. Introduction

The elastic/plastic buckling of plate, widely used in aerospace, mechanical, civil and marine engineering structures are concerned by many of the engineers. Moreover, plates are extensively used in structures such as aircraft wings and bridges. Then it is important to know buckling capacities of the structures in order to avoid premature failure. For large amounts of loading the buckling phenomena may occur in the plastic range. This phenomenon may be likely to occur in the cases of plates whose materials posses a low proportional limit when compared to the nominal yield stress, for example aluminum alloy and stainless steel. Researchers have given considerable attention to the buckling of plates issue numerically and analytically in both elastic and plastic buckling modes. They have investigated the plastic buckling behavior of plates subjected to uniaxial and biaxial compression loadings using two theories of strain-hardening plasticity, incremental and deformation theories. It would be useful for the design profession if a simple computing algorithm is available, that is rapidly adaptable to specific problems in determining the plastic bifurcation buckling loads.

Ilyushin [15], Handelman and Prager [13], Stowell [26] and Pride and Heimerl [18] carried out the plastic buckling analysis with incremental and deformation theories, respectively. They showed that the results attained by DT are close to the experimental results. Tugcu [28] illustrated that the analysis based on IT is more sensitive than DT with the test parameters. Geier and Singh [11] presented a simple analytical solution for computing bifurcation buckling loads of thin and moderately thick orthotropic cylindrical shells and panels subjected to axial compression and normal pressure. The analysis was based on the governing nonlinear equations. Durban [8] found out that the IT could predict more buckling load in comparison with DT, and that the experimental data had more congruence with DT. Of course, there are some cases where the critical stresses obtained from two theories are nearly equal. A typical example is furnished by axially symmetric buckling of axially compressed circular cylindrical shells. Durban and Zuckerman [9] carried out the analysis of rectangular plates under uniaxial loading for several various modes with the separation of variables solution. However, the limited boundary conditions consisting of clamped and simply supported have limited the obtained data in that research. If all boundary conditions are clamped, then it would

* Corresponding author. Tel.: +98 9153111869; fax: +98 5118763304.
E-mail address: kadkhoda@um.ac.ir (M. Kadkhodayan).

1270-9638/$ – see front matter
http://dx.doi.org/10.1016/j.ast.2013.12.003

Nomenclature

a, b	Plate lengths in x- and y-directions, respectively
$C_{ij}^{(1)}, C_{ij}^{(2)}, C_{ij}^{(3)}, C_{ij}^{(4)}$	The weighting coefficients of the first, second, third and fourth-orders
n, k	Ramberg–Osgood parameters
D	Flexural rigidity of plate $[\equiv Eh^3/12(1-\upsilon^2)]$
E	Young's modulus of elasticity
G	Effective shear modulus
h	Thickness of plates
h/a	Thickness to length ratio
K	Buckling coefficient $[\equiv Pa^2h/\pi^2 D]$
N_x, N_y	Number of grid point in the x- and y-directions, respectively
P_0	The maximum intensity of compressive force at the edge of plate in Eq. (29)
P_x	In-plane compressive forces per unit length of the plate in the x direction in Eq. (29)
S_{ij}	Stress deviator tensor
$S(E_s)$	Secant modulus
$T(E_t)$	Tangent modulus
U	Strain energy
V	Potential energy
w	Transverse deflection of the plate
X, Y, W	Non-dimensional parameters

Greek symbols

$\alpha, \beta, \gamma, \chi, \mu, \delta$	Parameters used in stress–strain relations
η	Loading parameter in Eq. (29)
ε_e	Total effective strain
ε	Total strain
λ	Aspect ratio $[\equiv a/b]$
υ	Poisson's ratio
σ_e	Effective stress
ξ	Loading ratio

be difficult to solve the problem and other numerical methods have to be used. In the present study, it is aimed to solve all these restrictions through generalized differential quadrature method.

Betten and Shin [6] showed that if the plate is slender, the buckling is elastic. However, if the plate is sturdy, it buckles in the plastic range and the instantaneous moduli in the constitutive equations depend on the external loading. Wang et al. [31,32,29] investigated the elastic–plastic buckling of thin and thick plates based on deformation and incremental theories by use of separation of variables and Ritz method. They came to the conclusion that the DT predicts less buckling stress factor, and as the thickness and Ramberg–Osgood constant increase, the differences between two theories increase. Smith et al. [25] studied the inelastic buckling of steel plates based on classical theory under different loading conditions by using Rayleigh–Ritz method. El-Sawy et al. [10] have employed the finite element method (FEM) to determine the elasto–plastic buckling stress of uniaxially loaded square and rectangular plates with circular cutouts. They showed that the critical buckling stress for perforated plates always decreases as the plate slenderness ratio increases and that this decrease becomes steeper for larger values of plate slenderness ratios, especially for small hole sizes where the failure changes from elasto–plastic into pure elastic. Grognec and Van [12] used the 3D plastic bifurcation theory assuming the incremental theory of plasticity with the von Mises yield criterion and a linear isotropic hardening. Wang et al. [30,34] studied the elastic/plastic buckling of thick and thin plates by differential quadrature method and confirmed the results of Refs. [9,31]. Aydin Komur [2] studied the effect of plate aspect ratio, elliptical hole size, angle and location and slenderness ratio on buckling behavior. He found that as the plate slenderness ratio increases, the critical buckling stress decreases for all perforated plates.

More recently, Robert et al. [20] compared the incremental and deformation theories and flow rules in simulating the sheet-metal forming processes. It can be concluded that the major advantage of the new approach was the time benefit when the material non-linearities were dominant. Weißgraeber et al. [33] studied the buckling behavior of an orthotropic plate with elastic clamping and edge reinforcement under uniform compressive load. Rahimi et al. [19] analyzed the buckling behavior of thin-walled cylindrical shells under axial force by finite element analysis method. They showed that stiffening the shells increased the buckling load while decreased the buckling load to weight ratio of an unstiffened shell.

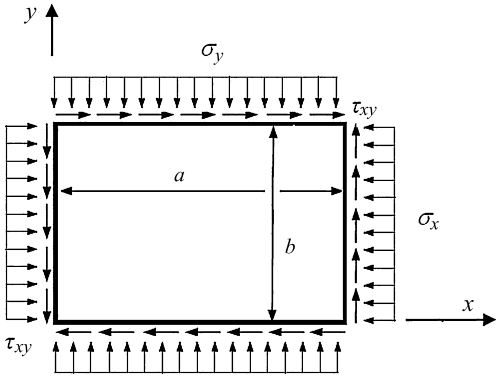

Fig. 1. Geometry and loading conditions of a rectangular plate.

Ruocco and Mallardo [21] applied a model to predict the buckling behavior of thin, orthotropic, stiffened plates and shells subjected to axial compression. The equilibrium equations have been solved applying the Kantorovich method. They showed that the Von Karman model could sensibly overestimate the critical load. Chakrabarty [7] pointed out the difference between bifurcation and stability and presented the equations used for the analyses. However, the point that the differences between the obtained results from two theories of deformation and incremental are observable is still a paradox.

In this work, details of elastic/plastic buckling of thin rectangular plates using incremental and deformation theories of plasticity are introduced first. An important criterion for sizing and certification of aircraft fuselages is the local and global buckling behavior. Therefore it is necessary to know the buckling behavior as accurately as possible. The uniform and non-uniform in-plane axial and biaxial tension/compression loadings with various boundary conditions are considered for the first time. The material properties described by the stress–strain relationship proposed by the Ramberg–Osgood stress–strain model. The GDQ method as an efficient numerical tool is employed to establish an eigenvalue problem and to calculate the plate buckling coefficients. The validation of the GDQ solutions by comparison with corresponding results for a typical aerospace aluminum alloy (AL 7075-T6) material is described. The numerical results are presented to show the effect of aspect, thickness to length and loading ratios, boundary condition, type of plasticity theory and linearly varying in-plane loading on the buckling coefficient of plates.

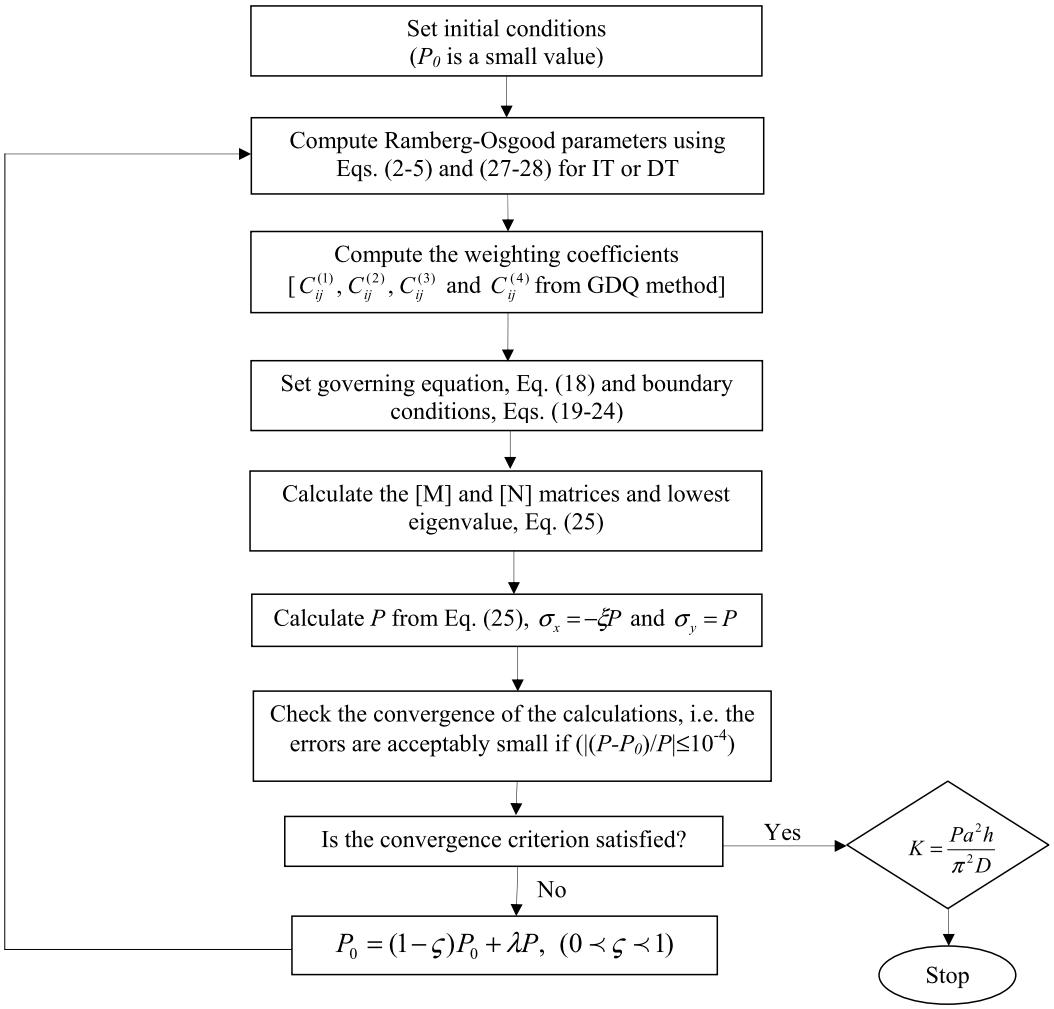

Fig. 2. The flow chart of calculation method.

2. Governing equations and boundary conditions

Fig. 1 shows the governing geometry on rectangular plates under in-plane uniform compressive stress and shear stress where a is the length, b is the width and h is the thickness of plate.

2.1. Equations from plasticity

The stress rate corresponding to strain rate in plate are given by:

$$\begin{Bmatrix} \dot{\sigma}_x \\ \dot{\sigma}_y \\ \dot{\tau}_{xy} \end{Bmatrix} = E \begin{bmatrix} \alpha & \beta & \chi \\ & \gamma & \mu \\ sym & & \delta \end{bmatrix} \begin{Bmatrix} \dot{\varepsilon}_x \\ \dot{\varepsilon}_y \\ \dot{\gamma}_{xy} \end{Bmatrix}, \tag{1}$$

where E is the Young modulus and α, β, γ, δ, μ and χ depend on the plasticity theory. There are two theories of plasticity used in this paper, IT based on Prandtl–Reuss equation and DT based on Hencky equation. The main difference between these two theories is that IT depends on incremental plastic strain and DT depends on total strain (see Appendix A).

According to incremental theory, the parameters α, β, γ, δ, μ, χ and G are given by [29]:

$$\alpha = \frac{1}{\rho}[c_{22}c_{33} - c_{23}^2], \qquad \beta = \frac{1}{\rho}[c_{13}c_{23} - c_{12}c_{33}],$$
$$\gamma = \frac{1}{\rho}[c_{11}c_{33} - c_{13}^2], \qquad \mu = \frac{1}{\rho}[c_{12}c_{13} - c_{11}c_{23}],$$
$$\chi = \frac{1}{\rho}[c_{12}c_{23} - c_{13}c_{22}], \qquad \delta = \frac{1}{\rho}[c_{11}c_{22} - c_{12}^2],$$
$$\rho = \frac{E}{T}\begin{vmatrix} c_{11} & c_{12} & c_{13} \\ c_{21} & c_{22} & c_{23} \\ c_{31} & c_{32} & c_{33} \end{vmatrix}, \qquad G = \frac{E}{2(1+\upsilon)}, \tag{2}$$

where

$$c_{11} = 1 - 3\left(1 - \frac{T}{E}\right)\left(\frac{\sigma_y^2}{4\sigma_e^2} + \frac{\tau_{xy}^2}{\sigma_e^2}\right),$$
$$c_{12} = -\frac{1}{2}\left[1 - (1-2\upsilon)\frac{T}{E} - 3\left(1 - \frac{T}{E}\right)\left(\frac{\sigma_x\sigma_y}{2\sigma_e^2} + \frac{\tau_{xy}^2}{\sigma_e^2}\right)\right],$$
$$c_{13} = \frac{3}{2}\left(1 - \frac{T}{E}\right)\left(\frac{2\sigma_x - \sigma_y}{\sigma_e}\right)\left(\frac{\tau_{xy}}{\sigma_e}\right),$$
$$c_{22} = 1 - 3\left(1 - \frac{T}{E}\right)\left(\frac{\sigma_x^2}{4\sigma_e^2} + \frac{\tau_{xy}^2}{\sigma_e^2}\right),$$
$$c_{23} = \frac{3}{2}\left(1 - \frac{T}{E}\right)\left(\frac{2\sigma_y - \sigma_x}{\sigma_e}\right)\left(\frac{\tau_{xy}}{\sigma_e}\right),$$
$$c_{33} = 2(1+\upsilon)\left(\frac{T}{E}\right) + 9\left(1 - \frac{T}{E}\right)\left(\frac{\tau_{xy}^2}{\sigma_e^2}\right). \tag{3}$$

According to deformation theory, the parameters $\alpha, \beta, \gamma, \delta, \mu$ and χ are calculated by employing Eqs. (A.3) and (2), and G in this theory is given by [29]:

$$G = E/\left[2 + 2\upsilon + 3\left(\frac{E}{S} - 1\right)\right] \tag{4}$$

where

$$c_{11} = 1 - 3\left(1 - \frac{T}{S}\right)\left(\frac{\sigma_y^2}{4\sigma_e^2} + \frac{\tau_{xy}^2}{\sigma_e^2}\right),$$

$$c_{12} = -\frac{1}{2}\left[1 - (1-2\upsilon)\frac{T}{E} - 3\left(1 - \frac{T}{S}\right)\left(\frac{\sigma_x\sigma_y}{2\sigma_e^2} + \frac{\tau_{xy}^2}{\sigma_e^2}\right)\right],$$

$$c_{13} = \frac{3}{2}\left(1 - \frac{T}{S}\right)\left(\frac{2\sigma_x - \sigma_y}{\sigma_e}\right)\left(\frac{\tau_{xy}}{\sigma_e}\right),$$

$$c_{22} = 1 - 3\left(1 - \frac{T}{S}\right)\left(\frac{\sigma_x^2}{4\sigma_e^2} + \frac{\tau_{xy}^2}{\sigma_e^2}\right),$$

$$c_{23} = \frac{3}{2}\left(1 - \frac{T}{S}\right)\left(\frac{2\sigma_y - \sigma_x}{\sigma_e}\right)\left(\frac{\tau_{xy}}{\sigma_e}\right),$$

$$c_{33} = 3\frac{T}{S} - (1-2\upsilon)\left(\frac{T}{E}\right) + 9\left(1 - \frac{T}{S}\right)\left(\frac{\tau_{xy}^2}{\sigma_e^2}\right). \tag{5}$$

2.2. Governing equation elastic/plastic buckling of thin plate

The strain energy functional for the plate is given by [7]:

$$U = \frac{1}{2}\int_V \{\dot\sigma_x\dot\varepsilon_x + \dot\sigma_y\dot\varepsilon_y + \dot\tau_{xy}\dot\gamma_{xy} + \dot\tau_{xz}\dot\gamma_{xz} + \dot\tau_{yz}\dot\gamma_{yz}\}\,dV. \tag{6}$$

The potential energy V for the plate subjected to uniform in-plane compressive and shear stress is given by:

$$V = -\frac{1}{2}\int_A \left(\dot\sigma_x h\left(\frac{\partial w}{\partial x}\right)^2 + \dot\sigma_y h\left(\frac{\partial w}{\partial y}\right)^2 + 2\dot\tau_{xy}h\left(\frac{\partial w}{\partial x}\right)\left(\frac{\partial w}{\partial y}\right)\right)dA. \tag{7}$$

Now, the principle of minimum total potential energy is used as:

$$\delta(U + V) = 0, \tag{8}$$

Table 1
The computational convergence rate for SSSS square plates under equibiaxial loading.

h/a	$N_x = N_y$					
	5	7	9	11	13	15
0.011	1.7832	2.0120	2.0010	2.0000	2.0000	2.0000
0.049	1.7375	1.8935	1.8880	1.8878	1.8878	1.8878

where δ represents the variational symbol. In order to simplify the parameter studies, the following non-dimensional variables are defined:

$$X = \frac{x}{a}, \qquad Y = \frac{y}{b}, \qquad \lambda = \frac{a}{b}, \qquad W = \frac{w}{a}. \tag{9}$$

Here, in the interest of brevity, only the final forms of the equilibrium equation for the elastic/plastic buckling of thin rectangular plate are presented in the dimensionless form as:

$$\begin{aligned}\alpha\frac{\partial^4 W}{\partial X^4} + 4\lambda\chi\frac{\partial^4 W}{\partial X^3\partial Y} + 2(\beta + 2\delta)\lambda^2\frac{\partial^4 W}{\partial X^2\partial Y^2} \\ + 4\mu\lambda^3\frac{\partial^4 W}{\partial X\partial Y^3} + \gamma\lambda^4\frac{\partial^4 W}{\partial Y^4} \\ = -\frac{12a^2}{h^2}\frac{\sigma_x}{E}\frac{\partial^2 W}{\partial X^2} - \frac{12a^2}{h^2}\lambda^2\frac{\sigma_y}{E}\frac{\partial^2 W}{\partial Y^2} \\ - \frac{24a^2}{h^2}\lambda\frac{\tau_{xy}}{E}\frac{\partial^2 W}{\partial X\partial Y},\end{aligned} \tag{10}$$

in which the parameters α, β, γ, δ, μ, χ are given by Eqs. (2)–(5).

2.3. Boundary conditions

To complete the formulation of the problem, the governing equations are accompanied by a set of boundary conditions. The boundary conditions are considered as follows.

– *Simply supported edge* (S)

The boundary conditions for simply supported edge $X = 0, X = 1$ are:

$$W = 0, \qquad \alpha\frac{\partial^2 W}{\partial X^2} + \beta\lambda^2\frac{\partial^2 W}{\partial Y^2} = 0 \tag{11}$$

and in $Y = 0$, $Y = 1$

$$W = 0, \qquad \gamma\lambda^2\frac{\partial^2 W}{\partial Y^2} + \beta\frac{\partial^2 W}{\partial X^2} = 0. \tag{12}$$

– *Clamped edge* (C)

The boundary conditions for clamped edge $X = 0, X = 1$ are:

$$W = 0, \qquad W_{,X} = 0 \tag{13}$$

and in $Y = 0$, $Y = 1$

$$W = 0, \qquad W_{,Y} = 0. \tag{14}$$

Table 2
Comparison studies of buckling coefficient for SSSS square thin plates under uniaxial and equibiaxial loadings with IT and DT predictions.

Type of loading	Sources	$h/a = 0.035$		$h/a = 0.049$	
		IT	DT	IT	DT
uniaxial	Ilyushin [15]	–	4.0000	–	2.8959
	Handelman and Prager [13]	4.0000	–	3.5740	–
	Stowell [26]	–	4.0000	–	2.6151
	Beleich [4]	–	4.0000	–	2.6548
	Kollbrunner [4]	–	4.0000	–	2.5827
	Shrivastava [22]	4.0000	4.0000	3.5278	2.8058
	Wang et al. [31]	4.0000	4.0000	3.4955	2.7954
	Wang and Aung [29]	4.0000	4.0000	3.4955	2.7954
	Present study	4.0000	4.0000	3.4955	2.7954
equibiaxial	Durban and Zuckerman [9]	2.0000	2.0000	1.8713	1.8649
	Wang et al. [31]	2.0000	2.0000	1.8713	1.8649
	Wang and Aung [29]	2.0000	2.0000	1.8713	1.8649
	Present study	2.0000	2.0000	1.8713	1.8649

– *Free edge* (F)

For a free $X=0$, $X=1$ edge, the boundary conditions are:

$$\alpha\frac{\partial^2 W}{\partial X^2}+\beta\lambda^2\frac{\partial^2 W}{\partial Y^2}=0,$$
$$\alpha\frac{\partial^3 W}{\partial X^3}+(\beta+2\mu)\lambda^2\frac{\partial^3 W}{\partial X\partial Y^2}=-\frac{12\sigma_x a^2}{Eh^2}\frac{\partial W}{\partial X} \quad (15)$$

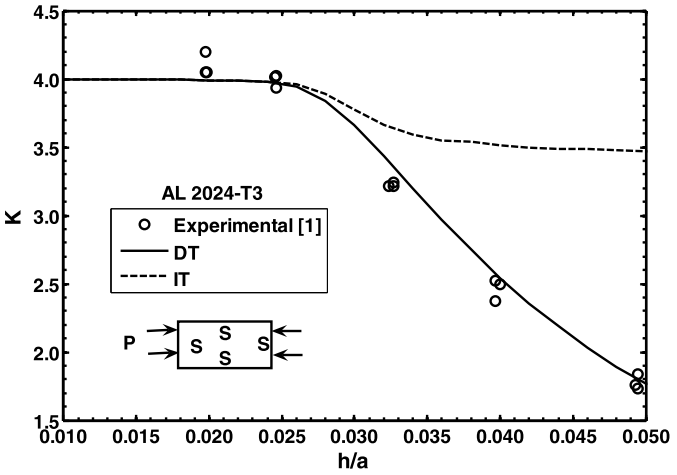

Fig. 3. Comparison of analytical results obtained by IT and DT with experimental results for SSSS square plate under uniaxial compression.

and in $Y=0$, $Y=1$

$$\gamma\lambda^2\frac{\partial^2 W}{\partial Y^2}+\beta\frac{\partial^2 W}{\partial X^2}=0,$$
$$\lambda^2\gamma\frac{\partial^3 W}{\partial Y^3}+(\beta+2\mu)\frac{\partial^3 W}{\partial X^2\partial Y}=-\frac{12\sigma_y a^2}{Eh^2}\frac{\partial W}{\partial Y}. \quad (16)$$

Durban and Zuckerman [9] have obtained analytical solutions for SSSS, SCSC and CSCS thin plates. But for the CCCC thin plate it was not possible to obtain a separation of variables solution. In the current study, it is tried to investigate the plastic buckling CCCC rectangular plate with various boundary conditions by using GDQ method for the first time.

3. GDQ analogs of the governing equation and boundary conditions

This method (GDQ) is practical and simple in solving engineering problems. It was used in 1971 by Bellman and Casti [3] as a new technique for numerical solving of ordinary or partial equations. Their purpose was to present a new way for overcoming the constant problems and amount of numerical problems. The first widespread use of this technique in the field of engineering problems was given by Bert and Malik [5]. The benefit of accessing to a new and exact solution with the least analyses in comparison to other numerical solutions like finite element and boundary element causes the efficiency of this method to be revealed gradually. This method can solve higher order differential equations with selecting few grid spacing. Its other characteristics are simple application, programming and high convergence rate [23,35].

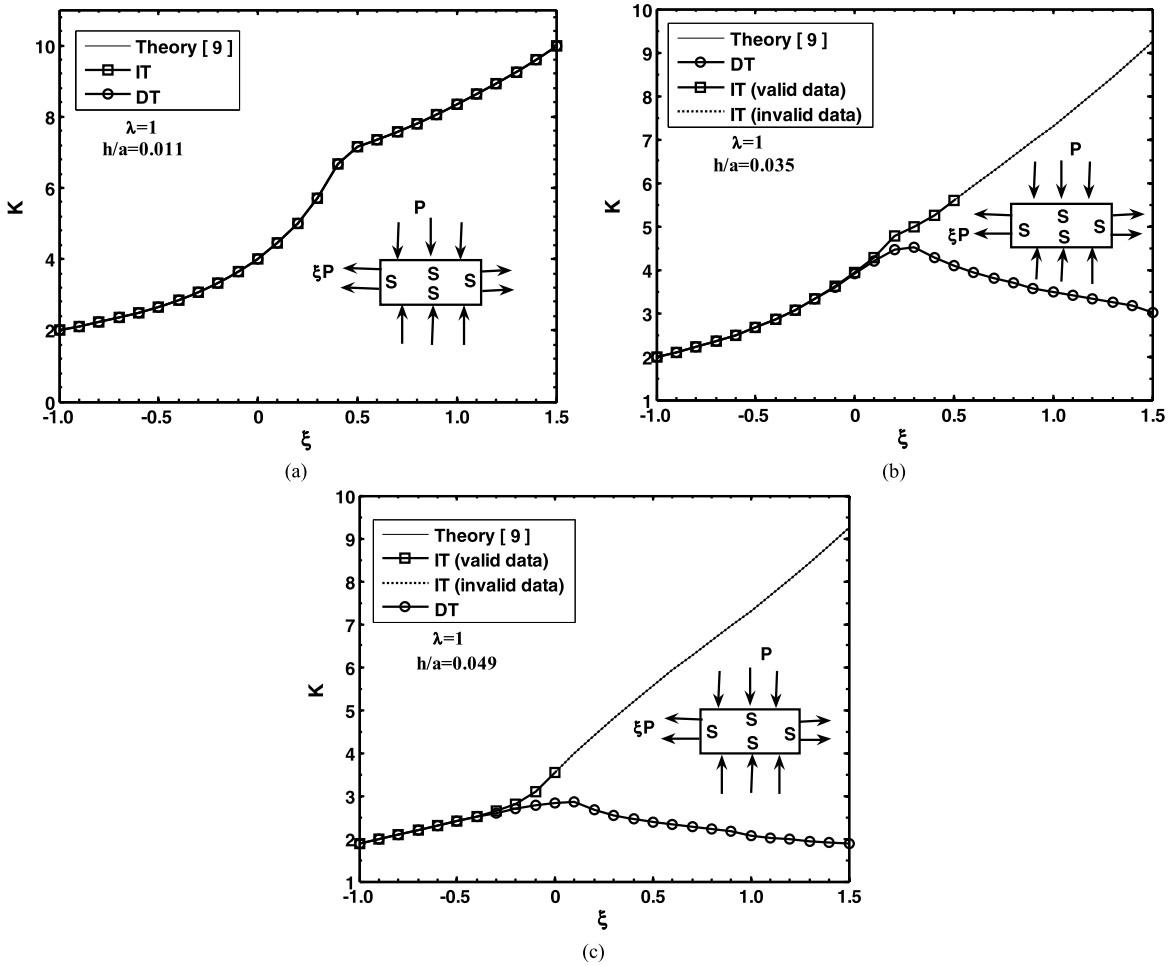

Fig. 4. Variations of buckling coefficient with loading and thickness to length ratios for SSSS square plates under IT and DT predictions.

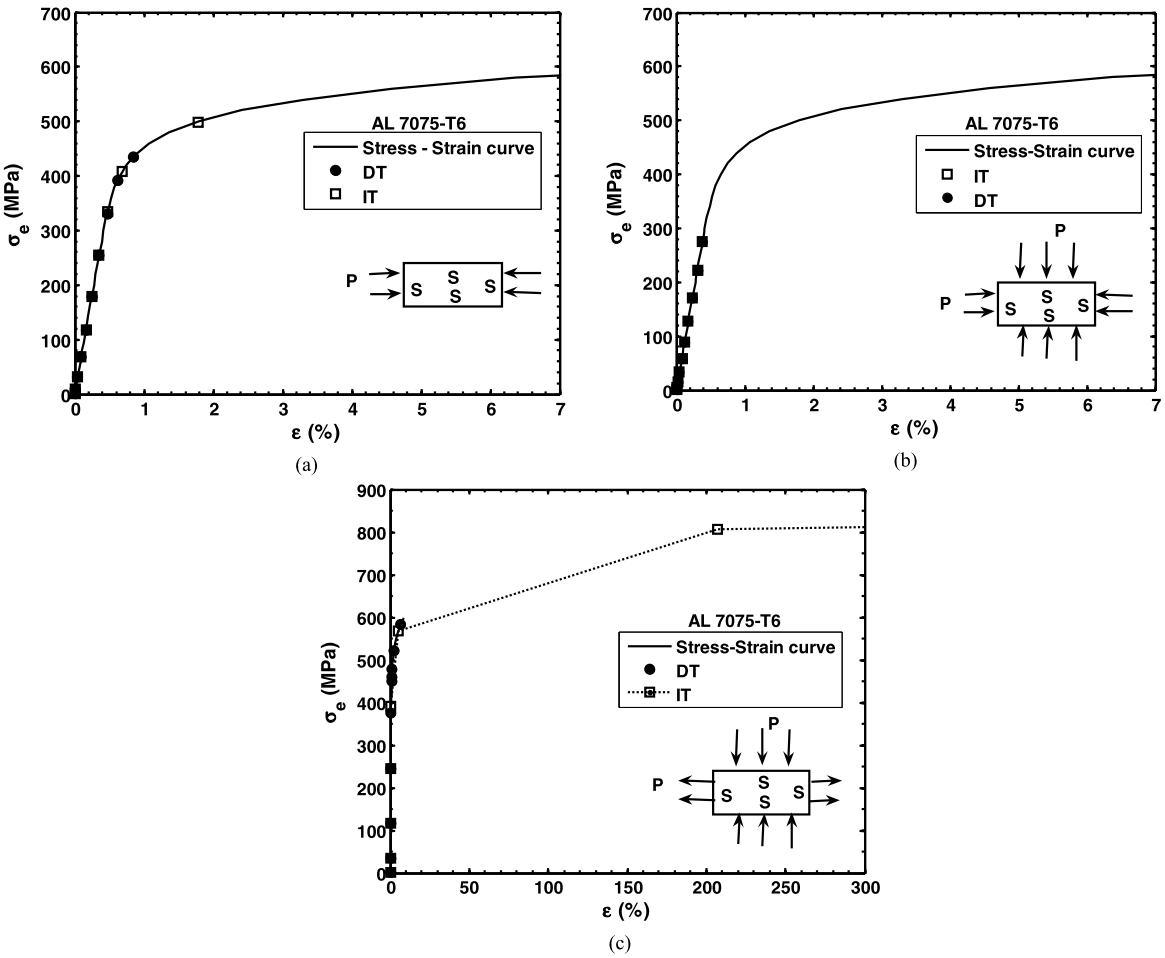

Fig. 5. The locations of IT and DT results on stress–strain curve for SSSS square plate under, (a) uniaxial compression, (b) equibiaxial compression and (c) equibiaxial tension/compression loadings ($0.0001 \leqslant h/a < 0.05$).

The GDQ discretization method has been adopted for the solution of elastic/plastic buckling of thin rectangular plate equations. The distributions of grid spacing of Chebyshev–Gauss–Lobatto (C-G-L) have the best convergence and highest accuracy [24]. In this study, the following relations are used:

$$x_i = \frac{1}{2}\left(1 - \cos\frac{i-1}{N_x - 1}\pi\right), \quad i = 1, 2, \ldots, N_x,$$
$$y_j = \frac{1}{2}\left(1 - \cos\frac{j-1}{N_y - 1}\pi\right), \quad j = 1, 2, \ldots, N_y. \tag{17}$$

According to the GDQ method, the governing Eq. (10) should also be re-written in discretized form. In terms of generalized differential quadrature, the governing differential equation at inner grid point is expressed by:

$$\begin{aligned}
&\alpha \sum_{k=1}^{N_x} C_{ik}^{(4)} W_{kj} + 2(\beta + 2\delta)\lambda^2 \sum_{m=1}^{N_y} C_{jm}^{(2)} \sum_{k=1}^{N_x} C_{ik}^{(2)} W_{km} \\
&\quad + 4\chi\lambda \sum_{m=1}^{N_y} C_{jm}^{(1)} \sum_{k=1}^{N_x} C_{ik}^{(3)} W_{km} \\
&\quad + 4\mu\lambda^3 \sum_{m=1}^{N_y} C_{jm}^{(3)} \sum_{k=1}^{N_x} C_{ik}^{(1)} W_{km} + \gamma\lambda^4 \sum_{k=1}^{N_y} C_{jk}^{(4)} W_{ik} \\
&= -\frac{12a^2}{h^2 E}\left(\sigma_x \sum_{k=1}^{N_x} C_{ik}^{(2)} W_{kj} + \lambda^2 \sigma_y \sum_{k=1}^{N_y} C_{jk}^{(2)} W_{ik}\right. \\
&\quad \left. + 2\lambda\tau_{xy} \sum_{m=1}^{N_y} C_{jm}^{(1)} \sum_{k=1}^{N_x} C_{ik}^{(1)} W_{km}\right), \\
&i = 3, 4, \ldots, N_x - 2, \quad j = 3, 4, \ldots, N_y - 2
\end{aligned} \tag{18}$$

where $C_{ij}^{(1)}$, $C_{ij}^{(2)}$, $C_{ij}^{(3)}$ and $C_{ij}^{(4)}$ are the weighting coefficients of the first, second, third and fourth-order derivatives with respect to x and y, W is the value of deflection and N_x, N_y are the number of grid points in the x and y-directions, respectively. Application of the GDQ method to the governing equations leads to a set of $(N_x - 2)^2 \times (N_y - 2)^2$ equations with the same number of unknowns for all nodes of the domain. With the aid of GDQ, the boundary conditions of Eqs. (11)–(16) can be shown as follows:

– *Simply supported edges in* $X = 0$, $X = 1$

$$\begin{aligned}
&W_{1j} = W_{N_x j} = 0, \quad j = 1, 2, \ldots, N_y, \\
&\alpha \sum_{k=1}^{N_x} C_{ik}^{(2)} W_{kj} + \beta\lambda^2 \sum_{n=1}^{N_y} C_{jn}^{(2)} W_{in} = 0, \quad i = 1, 2, \ldots, N_x
\end{aligned} \tag{19}$$

and in $Y = 0$, $Y = 1$

$$\begin{aligned}
&W_{i1} = W_{iN_y} = 0, \\
&\gamma\lambda^2 \sum_{n=1}^{N_y} C_{jn}^{(2)} W_{in} + \beta \sum_{k=1}^{N_x} C_{ik}^{(2)} W_{kj} = 0.
\end{aligned} \tag{20}$$

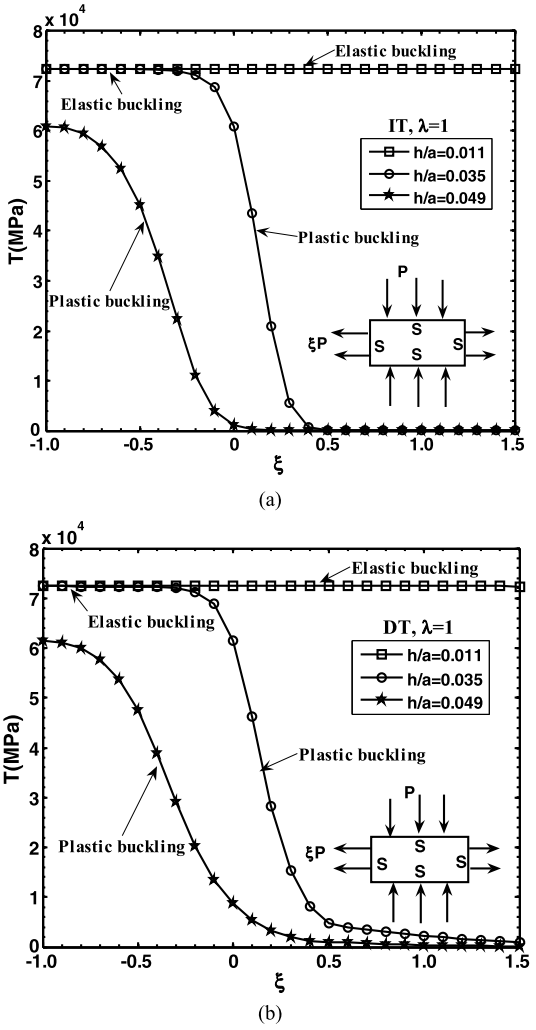

Fig. 6. Tangent modulus versus loading ratio by, (a) IT and (b) DT in various thicknesses parameters for SSSS square plate.

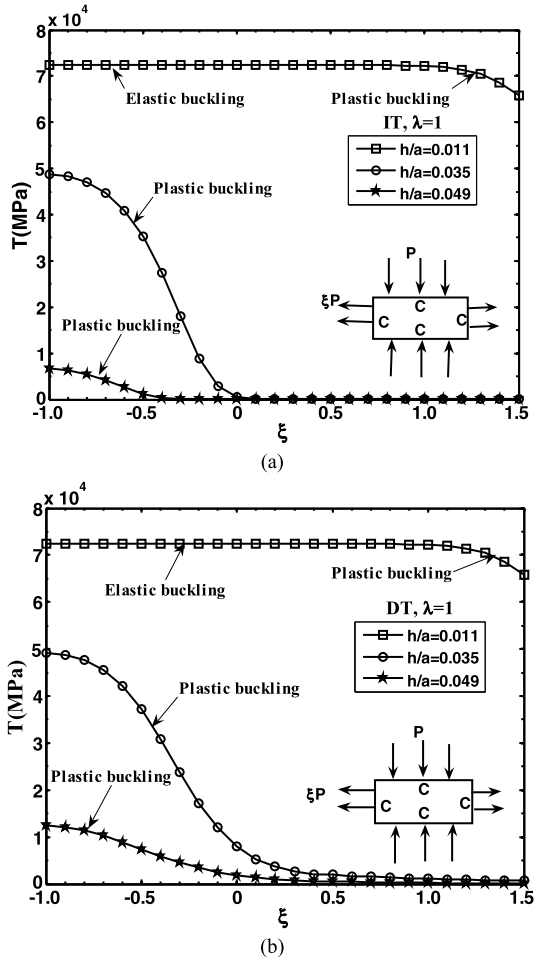

Fig. 7. Tangent modulus versus loading ratio by, (a) IT and (b) DT in various thicknesses parameters for CCCC square plate.

– *Clamped edges in* $X=0,\ X=1$

$$W_{1j}=W_{N_xj}=0,$$
$$\sum_{k=1}^{N_x}C_{ik}^{(1)}W_{kj}=\sum_{k=1}^{N_x}C_{N_xk}^{(1)}W_{kj}=0 \tag{21}$$

and in $Y=0,\ Y=1$

$$W_{i1}=W_{iN_y}=0,$$
$$\sum_{k=1}^{N_y}C_{k1}^{(1)}W_{ik}=\sum_{k=1}^{N_y}C_{kN_y}^{(1)}W_{ik}=0. \tag{22}$$

– *Free edges in* $X=0,\ X=1$

$$\alpha\sum_{k=1}^{N_x}C_{ik}^{(2)}W_{kj}+\beta\lambda^2\sum_{n=1}^{N_y}C_{jn}^{(2)}W_{in}=0,$$
$$(\beta+2\mu)\lambda^2\sum_{m=1}^{N_y}C_{jm}^{(2)}\sum_{k=1}^{N_x}C_{ik}^{(1)}W_{km}+\alpha\sum_{k=1}^{N_x}C_{ik}^{(3)}W_{kj}$$
$$=-\frac{12a^2\sigma_x}{h^2E}\left(\sum_{k=1}^{N_x}C_{ik}^{(1)}W_{kj}\right) \tag{23}$$

and in $Y=0,\ Y=1$

$$\beta\sum_{k=1}^{N_x}C_{ik}^{(2)}W_{kj}+\gamma\lambda^2\sum_{n=1}^{N_y}C_{jn}^{(2)}W_{in}=0,$$
$$(\beta+2\mu)\sum_{m=1}^{N_y}C_{jm}^{(1)}\sum_{k=1}^{N_x}C_{ik}^{(2)}W_{km}+\lambda^2\gamma\sum_{k=1}^{N_y}C_{jk}^{(3)}W_{ik}$$
$$=+\frac{12a^2\sigma_y}{h^2E}\left(\sum_{k=1}^{N_y}C_{jk}^{(1)}W_{ik}\right). \tag{24}$$

Assume that $\sigma_x=-\xi P$, $\sigma_y=P$ and $\tau_{xy}=0$. It is easily seen that the final equations of matrices, Eqs. (18)–(24), are a set of nonlinear eigenvalue equations with the size of $(N_x)^2\times(N_y)^2$. Eq. (18) yield the buckling coefficient (the lowest eigenvalue) by solving the generalized following eigenvalue problem:

$$[M][W]=\frac{12Pa^2}{Eh^2}[N][W], \tag{25}$$

where M and N are matrices derived from the governing equation (18). Now, the non-dimensional buckling coefficient, K can be defined as:

$$K=\frac{Pa^2h}{\pi^2D}, \tag{26}$$

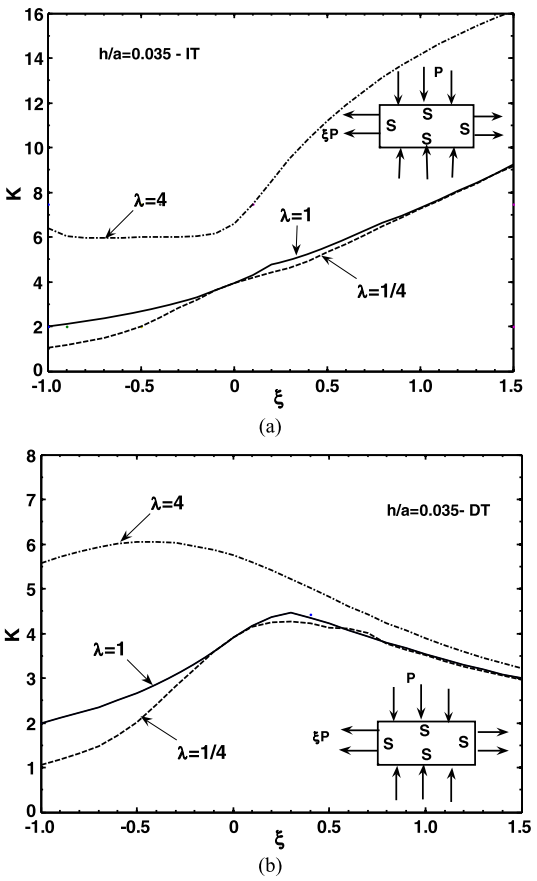

Fig. 8. Buckling coefficient versus loading ratio for SSSS rectangular plates subjected to various aspect ratios in $h/a = 0.035$.

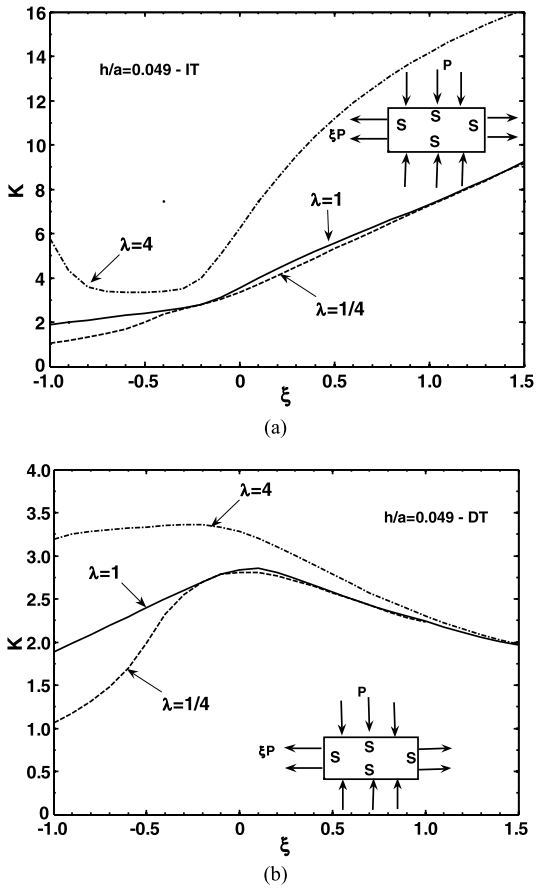

Fig. 9. Buckling coefficient versus loading ratio for SSSS rectangular plates subjected to various aspect ratios for $h/a = 0.049$.

where $D = Eh^3/12(1-\nu^2)$, is the plate flexural rigidity. Here the GDQ method as an efficient numerical tool is employed to solve these equations. Moreover, an iterative method should be used to solve the system of nonlinear eigenvalue Eq. (25). A computer program EBITP (Elastic/plastic Buckling of Isotropic Thin Plates) is developed based on the above mentioned formulation which is very quick and easy to generate elastic/plastic buckling coefficient of plate. The flow chart of GDQ method is briefly outlined in Fig. 2.

4. Mechanical properties of material and comparison studies

The material used in this study is a typical aerospace aluminum alloy (AL 7075-T6). The strain hardening plastic behavior of most structural materials used in aerospace and off-shore applications can be adequately described by the Ramberg–Osgood stress–strain relationship as follows:

$$\varepsilon = \frac{\sigma_e}{E} + k\left(\frac{\sigma_e}{E}\right)^n \tag{27}$$

where ε is the total strain and k and n are the material parameters. The tangent and secant moduli used in the equation are calculated as follows:

$$\frac{E}{T} = 1 + nk\left(\frac{\sigma_e}{E}\right)^{n-1}, \qquad \frac{E}{S} = 1 + k\left(\frac{\sigma_e}{E}\right)^{n-1}. \tag{28}$$

Consider a case that exhibits elastic/plastic material behavior, with the following parameters, Eq. (27): $E = 72.4$ GPa, $n = 10.9$, $k = 3.94 \times 10^{21}$ and Poisson's ratio $\nu = 0.32$ [9]. To increase the accuracy of the analysis the grid spacing has to be selected properly. Table 1 shows the convergence study for SSSS square plates under equibiaxial loading. If the grid points are increased from 11 to 15, the GDQ results will have no changes. Therefore, the numbers of grid points are selected as 11 ($N_x = N_y$). It is seen that the convergence rate of GDQ method is excellent. Table 2 shows the comparison studies of buckling coefficient for uniaxial and equibiaxial SSSS square plates. The present results for thickness to length of $h/a = 0.035$ and $h/a = 0.049$ were compared with results of other researchers. They are in good agreement and it is verified that the present GDQ solution is correct and accurate. A comparison between the obtained results and experimental data for rectangular plates under uniaxial compression are presented in Fig. 3. It can be seen that the results attained by DT which violates the fundamental rule of plastic flow of metal are close enough to the experimental ones.

5. Numerical results and discussions

In this section, the close form solutions of Eq. (10) for two types of uniform and linearly varying in-plane loadings are presented. Moreover, the effects of aspect, thickness to length and loading ratios, boundary conditions, type of plasticity theory and linearly varying in-plane loading on the buckling coefficient are discussed. Contour plots of buckling mode shapes for various loading parameters are also displayed.

5.1. Uniaxial and biaxial loadings

As it is shown in Fig. 1, when $\sigma_x = -\xi P$, $\sigma_y = P$ and $\tau_{xy} = 0$, the loading ratio $\xi = 1$ for biaxial compression/tension and $\xi = -1$ for the equibiaxial compression are considered. Moreover, if we

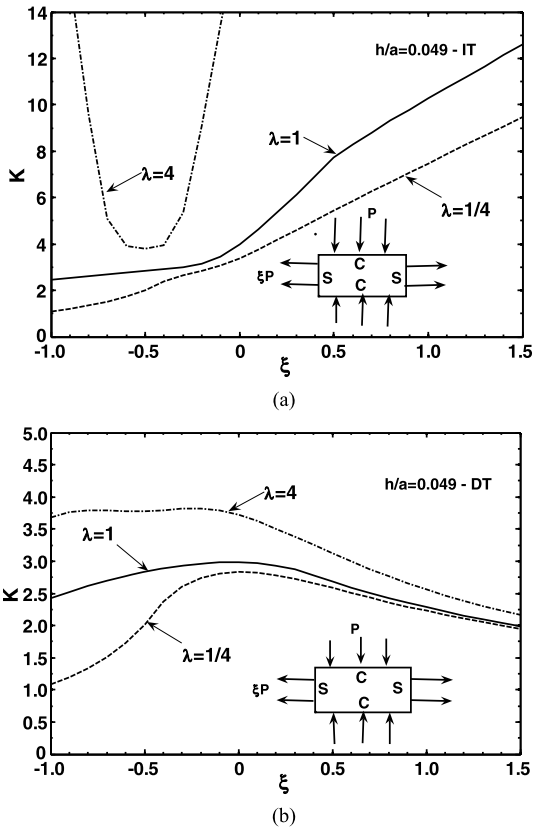

Fig. 10. Buckling coefficient versus loading ratio for SCSC rectangular plates subjected to various aspect ratios for $h/a = 0.049$.

have $\sigma_x = -\xi P$, $\sigma_y = 0$, $\tau_{xy} = 0$ and $\xi = -1$ the uniaxial compression is occurred.

5.1.1. Effect of loading ratio on the buckling coefficient

Firstly to verify the current study, some obtained results are compared with those of Ref. [9] and then some new results are presented. The buckling coefficient (K) in terms of loading ratio (ξ) for different thickness to length ratios (h/a) are calculated by incremental and deformation theories for SSSS plate, and it is observed that there is a good consistency between the current results and those of Ref. [9] for square plate, Fig. 4. In the case of square plate under biaxial compression, buckling occurs in elastic mode when $h/a = 0.011$ and the obtained results from incremental and deformation theories are in agreement with those of Ref. [9]. In this case and for all boundary conditions, the results for buckling coefficients are close to elastic buckling theory. When $h/a = 0.035$, $\xi < 0.1$ and $h/a = 0.049$, $\xi < -0.3$, there would be a good congruence between two theories of plasticity. However, with increasing the loading ratio in biaxial compression/tension, the differences increase too, Fig. 4.

In transverse tension and using DT, with increasing the loading ratio, the buckling coefficient decreases. In addition, the results obtained by IT and DT are closer to each other in biaxial compression, $-1 \leqslant \xi < 0$ rather than biaxial compression/tension, $0 < \xi \leqslant 1.5$. Furthermore, the differences between the results of two theories become more when the thickness to length ratio increases. In some cases, the elastic/plastic buckling coefficient predictions are not placed on stress–strain curve which are shown by dash lines. The results of IT placed on stress strain curve are shown by square lines. Therefore, the IT predicts some incorrect results.

Fig. 5 illustrates the locations of IT and DT results on stress–strain curve for SSSS square plate under (a) uniaxial compression,

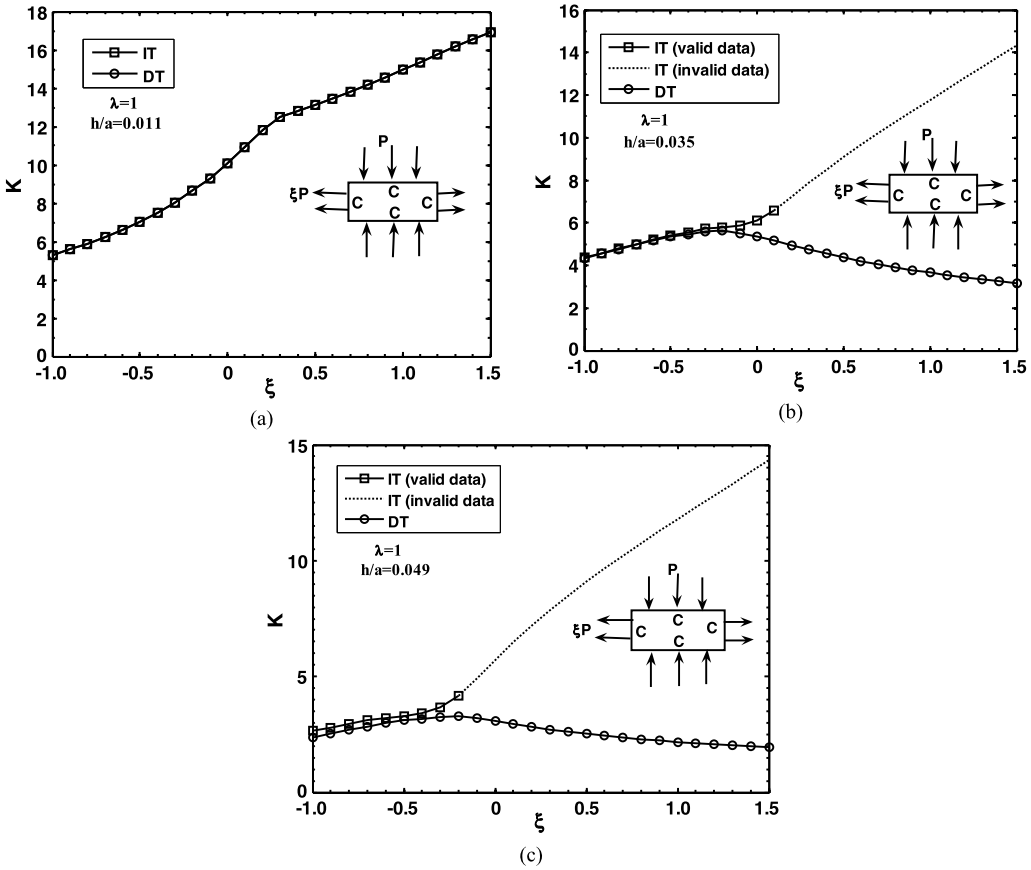

Fig. 11. Variations of buckling coefficient with loading and thickness to length ratios for CCCC square plates under IT and DT predictions.

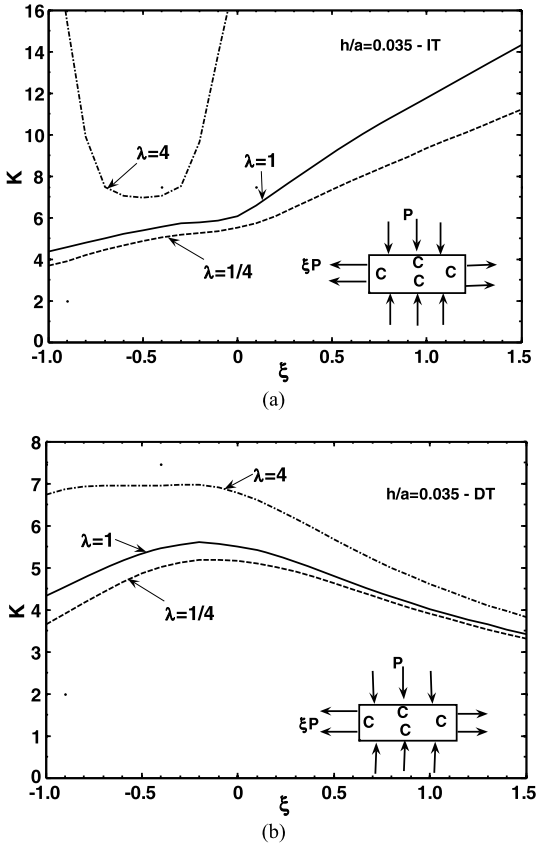

Fig. 12. Buckling coefficient versus loading ratio for CCCC rectangular plates subjected to various aspect ratios for $h/a = 0.035$.

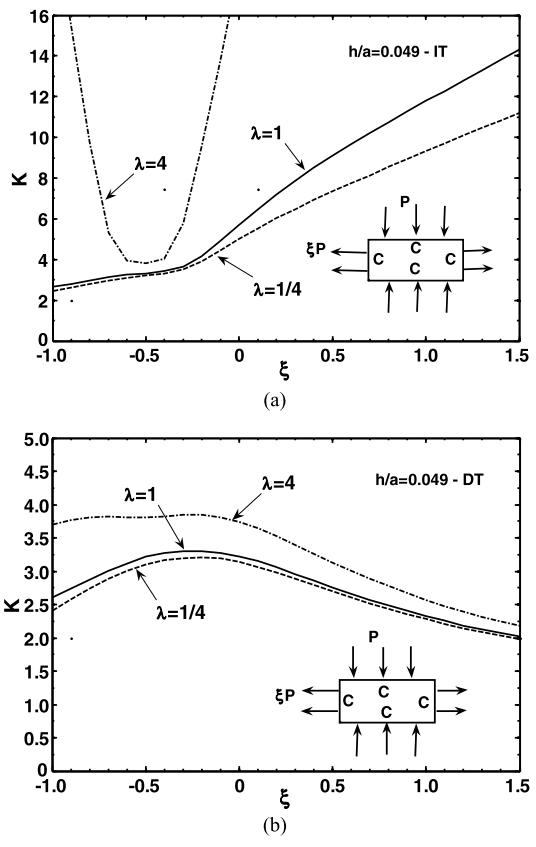

Fig. 13. Buckling coefficient versus loading ratio for CCCC rectangular plates subjected to various aspect ratios for $h/a = 0.049$.

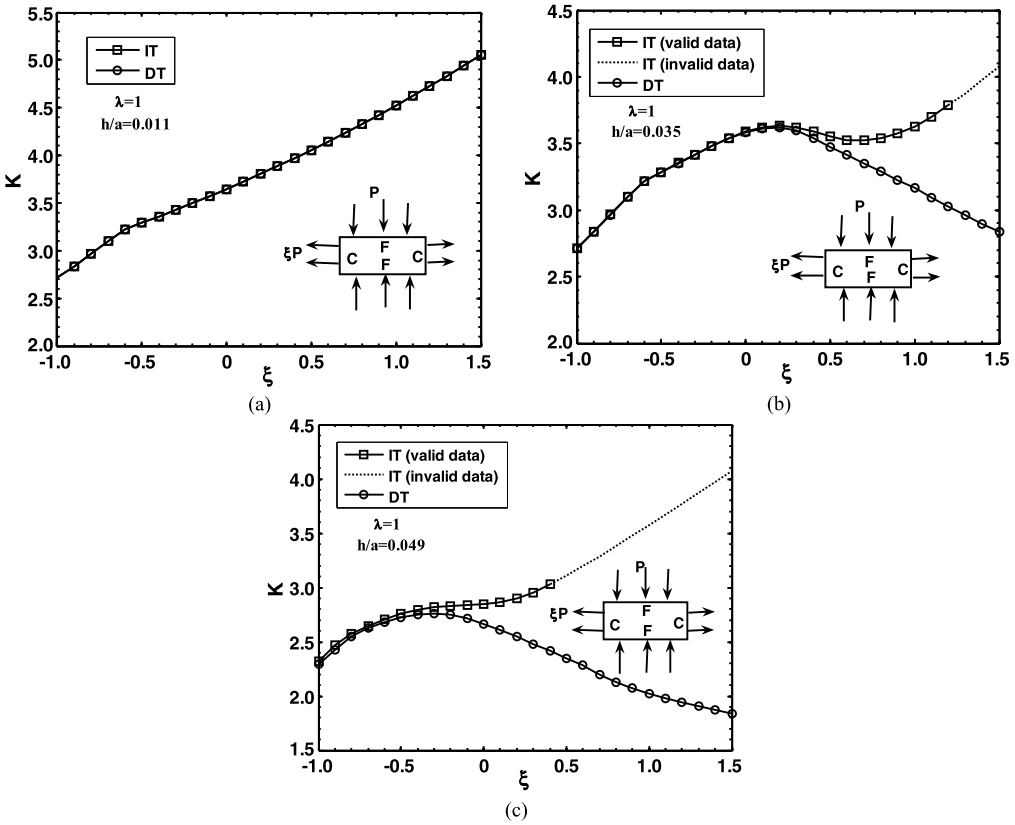

Fig. 14. Variations of buckling coefficient with loading and thickness to length ratios for CFCF plates under IT and DT predictions.

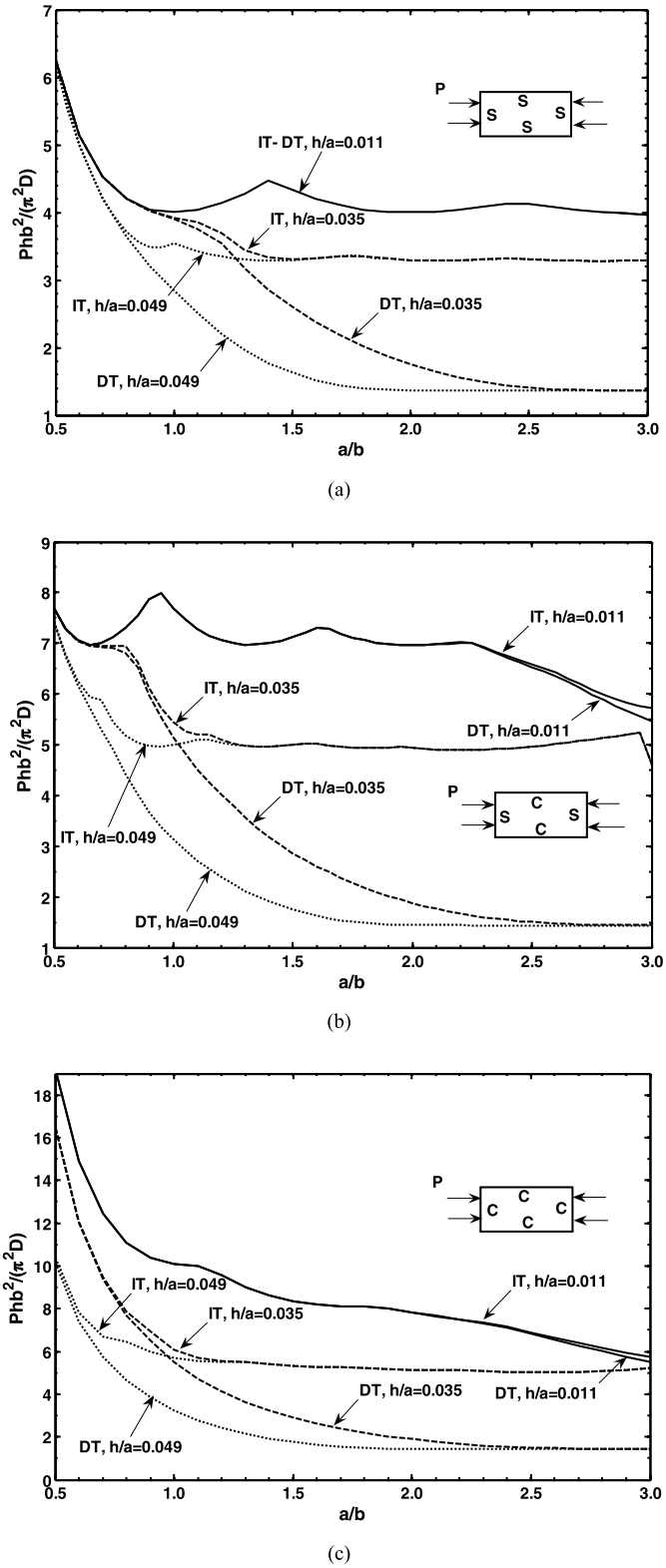

Fig. 15. Variations of buckling coefficient, $Phb^2/\pi^2 D$, with aspect and thickness to length ratios for rectangular plate under various boundary conditions, uniaxial loading and IT and DT predictions.

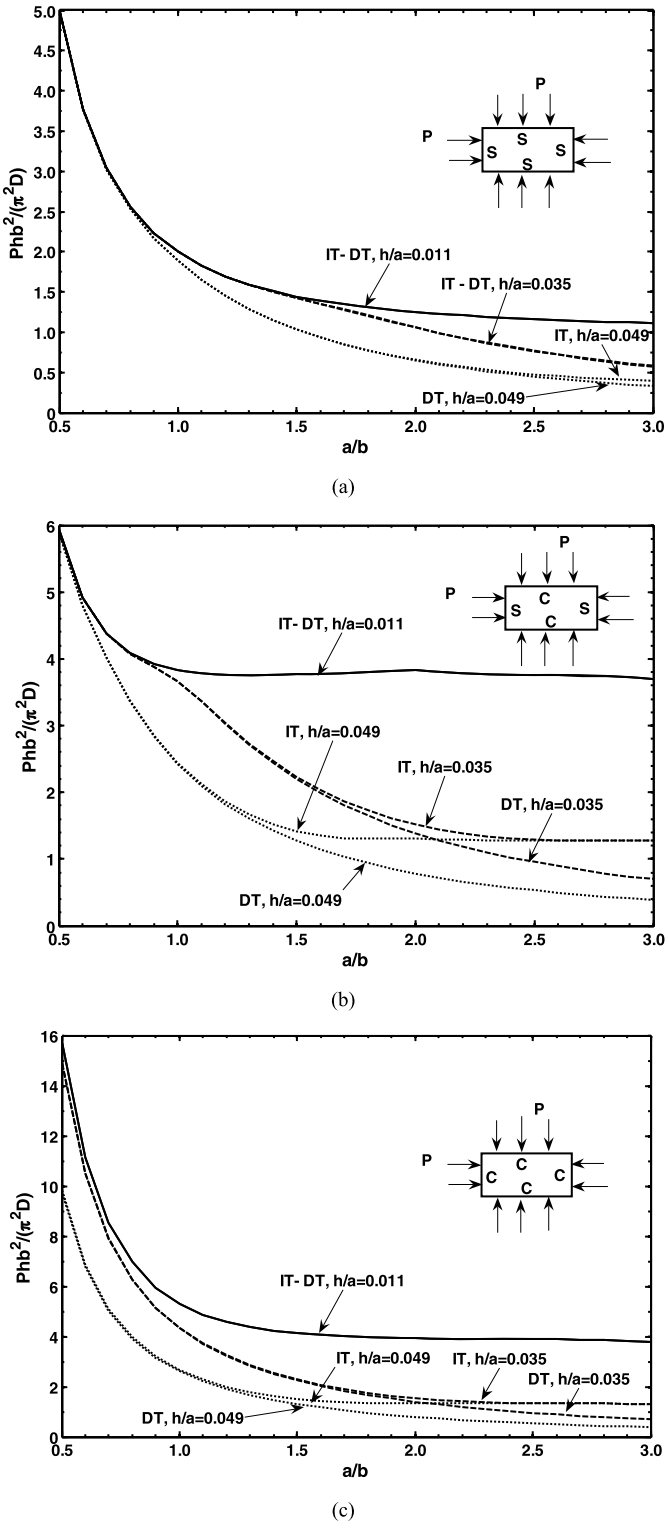

Fig. 16. Variations of buckling coefficient, $Phb^2/\pi^2 D$, with aspect and thickness to length ratios for rectangular plate under various boundary conditions, equibiaxial loading and IT and DT predictions.

(b) equibiaxial compression and (c) equibiaxial compression/tension loadings in $0.0001 \leqslant h/a < 0.05$. As it is seen, the IT and DT results coincide on stress–strain curve of AL 7075-T6 in uniaxial and equibiaxial loadings, Figs. 5(a) and 5(b). It has to be mentioned that unlike the uniaxial and equibiaxial loadings, the results stand out of stress–strain curve with increasing the thickness to length ratio in biaxial compression/tension loading and IT has predicted invalid data.

The behavior of the tangent modulus, T, against loading ratio, ξ, for the SSSS square plate is shown in Fig. 6 for various thickness to length ratios and incremental and deformation theories. While the thickness to length ratio is $h/a = 0.011$, elastic buckling and

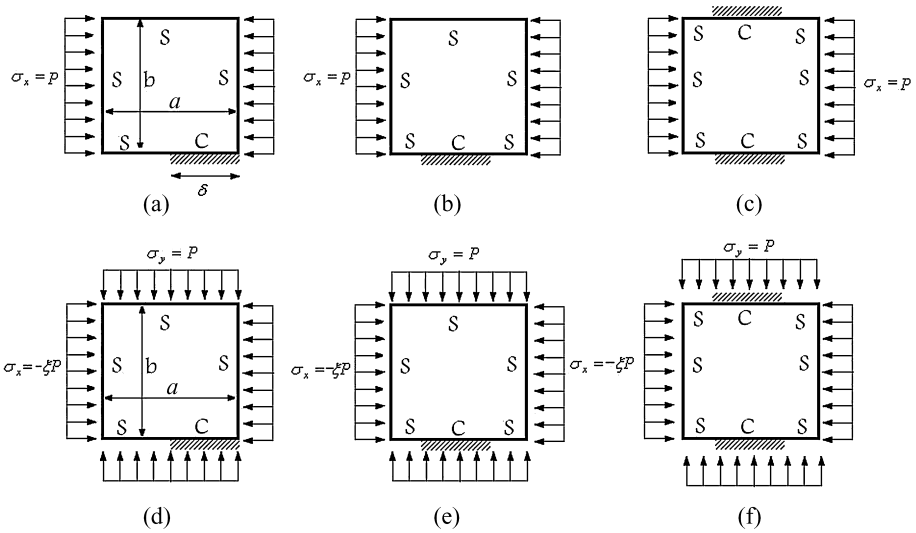

Fig. 17. Mixed boundary conditions under various loadings.

when they are $h/a = 0.035$ and 0.049, elastic–plastic and plastic buckling occur, respectively. Increasing of plastic zone leads to reduction of plate stiffness and decreases the buckling coefficient. It can be figured out from Fig. 6 that with increasing of thickness to length and loading ratios in biaxial compression/tension, the tangent modulus, T, becomes zero under incremental prediction which shows the results obtained from this theory cannot be admissible. Comparing Figs. 6 and 7 shows that with increasing thickness to length ratio in CCCC square plate the plastic buckling occurs earlier. Hence, in SSSS and CCCC square plates when $h/a = 0.035$ and $-1 \leqslant \xi \leqslant -0.3$ the elastic and plastic buckling occur under IT and DT predictions, respectively. By increasing the loading ratio and thickness of plate, the plasticity in plate increases and the discrepancy between instantaneous moduli of two theories increases.

5.1.2. Effect of aspect ratio on the buckling coefficient

Fig. 8 shows the curve of loading ratio in terms of buckling coefficient in various aspect ratios for both incremental and deformation theories in SSSS rectangular plate in $h/a = 0.035$. The results are the same as those reported by Durban and Zuckerman [9]. As aspect ratio increases, the buckling coefficient also increases. Similar behavior is observed for different boundary conditions and thickness to length ratio, Figs. 9 and 10. In analyses by DT, as the thickness to length ratio increases, the effect of aspect ratio on buckling coefficient in biaxial compression ($-1 \leqslant \xi < 0$) and biaxial compression/tension ($0 < \xi \leqslant 1.5$) decrease which is near to the experimental results [26,4,22]. Moreover, in biaxial compression, with increasing the thickness to length ratio the buckling coefficient decreases and the rate of reduction increases when higher aspect ratio is used, Figs. 8 and 9.

Fig. 10 shows the variations of buckling coefficient with in-plane load ratio for SCSC rectangular plate. It is seen that generally the buckling coefficient increases with increasing of aspect ratio. In biaxial compression/tension loading, the buckling coefficient increases with increasing of loading ratio in IT and decreases steadily in DT. When IT is used, the buckling coefficient tends infinity with increasing the loading ratio as the in-plane loading changes from biaxial compression to biaxial compression/tension which shows the results achieved from IT are not admissible. For the CCCC rectangular plates, however, Durban and Zuckerman [9] could not obtain a separation of variable solution for the eigenmodes. The elastic/plastic buckling of CCCC plate is analyzed here.

Table 3
Comparison studies of buckling coefficient for square plates with mixed boundary conditions, $h/a = 0.035$.

Case	δ	K		
		Mizusawa [17] (Spline element)	Wang and Aung [29] (Ritz method)	Present study (GDQ)
(a)	0	4.000	4.000	4.0000
	L/2	5.198	5.4654	5.4651
	L	5.740	5.7401	5.7401
(b)	0	4.000	4.0000	4.0000
	L/2	5.684	5.7252	5.7260
	L	5.740	5.7401	5.7401
(c)	0	4.000	4.000	4.000
	L/2	7.430	7.6217	7.6516
	L	7.690	7.6911	7.6913

It is clearly seen from Fig. 11 that with applying the clamped boundary conditions in all edges, the discrepancy between the results obtained from two plastic theories increase. In the CCCC boundary condition, when $h/a = 0.011$, elastic buckling and when thickness to length ratio increases, plastic buckling occur. Moreover, when $h/a = 0.0349$ and $\xi < -0.6$, there is a good congruency between two theories. But using clamped conditions increase the stresses in the plates and the variations between two theories as in $h/a = 0.0493$ no congruency can be observed. When clamped boundary condition increases, buckling tends to happen in plastic mode, Fig. 11. It is clearly seen that with increasing the clamped boundary condition the range of valid data in IT prediction decreases, Figs. 4 and 11.

Figs. 12 and 13 show the variations of buckling coefficient versus aspect ratio for IT and DT results in CCCC rectangular plate for $h/a = 0.0349$ and $h/a = 0.0493$, respectively. It is seen that using IT and clamped boundary condition, the buckling coefficient increases sharply with increasing the aspect ratio.

Fig. 14 displays the comparison between the buckling coefficient of incremental and deformation theories for CFCF square plate with various thickness to length ratios. With increasing the free boundary conditions, the discrepancy between the results of IT and DT and the buckling coefficients decrease, Figs. 11 and 14.

Figs. 15 and 16 illustrate the variations of buckling coefficient with aspect and thickness to length ratios for uniaxial and equibiaxial loadings under various boundary conditions. It can be observed that there is a good agreement between the re-

sults of IT and DT predictions in uniaxial loading for $h/a = 0.011$. However, with increasing the thickness to length ration the discrepancy increases. In equibiaxial loading, there are more agreements between IT and DT results rather than in uniaxial loading, Fig. 16.

5.1.3. Effect of boundary conditions on the buckling coefficient

A plate under mixed boundary conditions is shown in Fig. 17. In order to verify the correctness of the method, comparison studies are shown in Table 3 for three different cases. The value of $h/a = 0.035$ is adopted in the analyses in order to compare the results with the existing elastic buckling ones. The elastic buckling analysis can readily be obtained from a plastic buckling analysis by setting $(E = T = S)$. It is obvious that the present buckling coefficients agree very well with the analytical results. Fig. 18 shows the variations of the buckling coefficient K against the loading ratio, ξ, for square plates under mixed boundary conditions (Figs. 17(d) to 17(f)) for $h/a = 0.049$. It is seen that with increasing of clamped boundary conditions in any edges, the buckling coefficient increases. The increase is more observable in IT rather than DT.

5.2. Linearly varying in-plane loading

Plates are a part of complex structural system loads may not be always uniform, i.e. the load exerted on the aircraft wings usually is non-uniform. To the best of author's knowledge, no work has been reported concerned with the plastic buckling of plate under linearly varying in-plane loading. Hence, this part of present paper is concerned with this type of loading. Related to the in-plane stresses $(\sigma_x, \sigma_y, \tau_{xy})$, $P_x = \sigma_x h$, $P_y = \sigma_y h$ and $P_{xy} = \tau_{xy} h$. Let us assume $P_y = P_{xy} = 0$ and express P_x by:

$$P_x = -P_0\left(1 - \eta\frac{y}{b}\right), \tag{29}$$

where P_x is the in-plane compressive forces per unit length of the plate in the x-direction, P_0 is the maximum intensity of compressive force at the edge of plate and η is the loading parameter. By changing η, one can obtain various particular cases, as shown in Fig. 19, i.e. $\eta = 0$ for uniaxial compressive force, $\eta = 1$ for compressive force, force varies linearly from $-P_0$ at $y = 0$ to zero at $y = b$, and $\eta = 2$ for pure in-plane bending, occurs. For other values of η taken within 0 and 2, there is a combination of bending and compression. In order to check the accuracy of the results, comparison studies are shown in Table 4 against existing elastic buckling results because there was no plastic buckling results available.

Table 5 indicates the results of analysis of buckling coefficients for plates under different thickness to length ratios and subjected to various in-plane loadings. As it is shown, the maximum variation of buckling coefficient occurs in thin plate under different loading parameters for $h/a = 0.011$. Moreover, as it is observed from Table 5, with increasing the loading parameter the buckling coefficient increases for various boundary conditions.

5.2.1. Effect of aspect ratio on the buckling coefficient

Figs. 20 to 22 show the variations of aspect ratio against buckling coefficient for different values of thickness to length ratios for $\eta = 0$ to $\eta = 2$ and various boundary conditions shown with solid and short dash lines for IT and DT, respectively. The buckling coefficient increases as the loading parameter changes from uniaxial compressive $(\eta = 0)$ to pure in-plane bending $(\eta = 2)$. As it is clear, the more variations occur in the interval of $a/b < 1$, however; for the values of $a/b > 1$ the buckling coefficients remain almost constant. Moreover, the concurrence

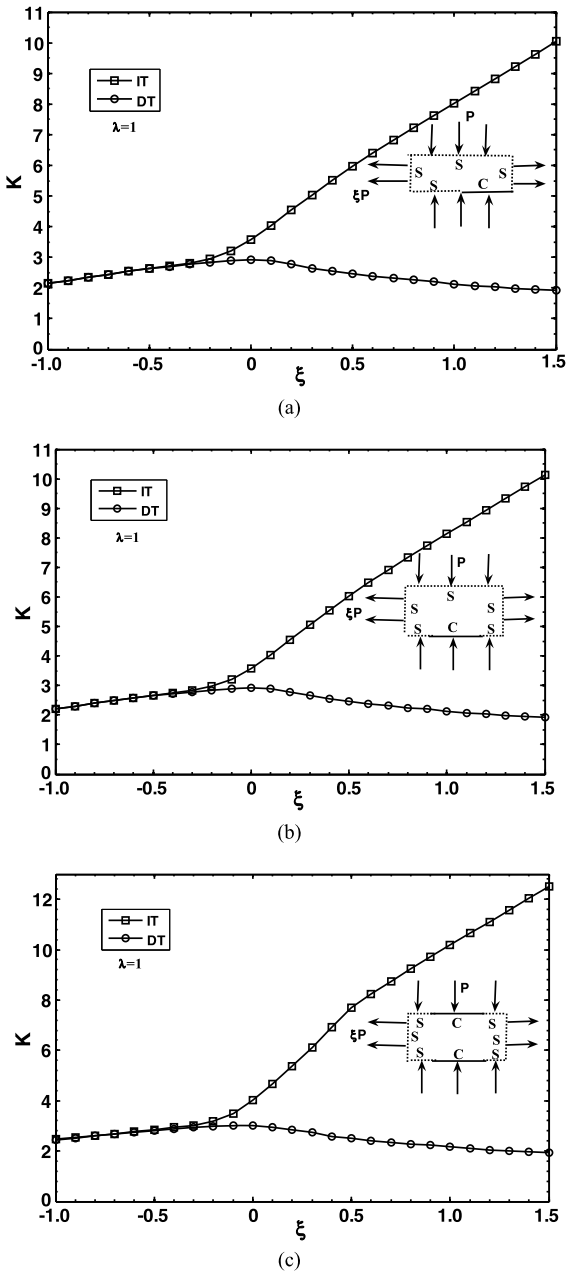

Fig. 18. Variations of buckling coefficient with loading ratio for SSSS square plates under mixed boundary conditions with the aid of IT and DT.

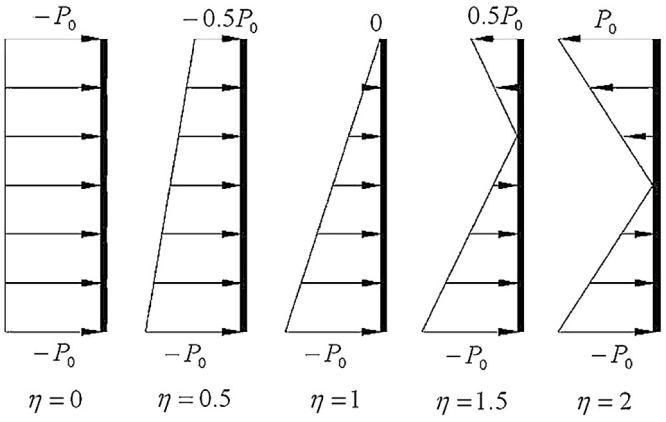

Fig. 19. Example of in-plane loading $P_x = -P_0(1 - \eta\frac{y}{b})$ along the edges $X = 0$, 1.

Table 4
Comparison studies of the buckling coefficient for SSSS and SCSC square thin plates $h/a = 0.011$ subjected to various in-plane loadings.

B.C	Sources	Method	η				
			0	0.5	1	1.5	2
SSSS	Leissa and Kang [16]	Exact solution	4.0000	5.3183	7.8118	13.3743	25.5329
	Timoshenko and Gere [27]	Energy	4.0000	–	7.8017	–	25.6342
	Hosseini et al. [14]	Ritz	4.0000	–	7.8119	–	25.528
	Present study	GDQ	4.0000	5.3183	7.8121	13.5139	25.5291
SCSC	Leissa and Kang [16]	Exact solution	7.6913	–	14.7118	–	39.6672
	Timoshenko and Gere [27]	Energy	7.6902	–	14.6915	–	39.7179
	Present study	GDQ	7.6913	10.2019	14.7131	23.4962	39.6748

Table 5
Comparison studies of the elastic/plastic buckling coefficient for square thin plates subjected to various in-plane loadings under different boundary conditions.

B.C	h/a	η				
		0	0.5	1	1.5	2
SSSS	0.011	4.0000	5.3183	7.8121	13.5139	25.5291
	0.035	3.9027	4.7459	5.6338	6.0661	7.8952
	0.049	2.8396	3.0582	3.0834	4.3938	7.0690
SSSC	0.011	5.7404	7.3488	10.1070	15.5600	25.5340
	0.035	4.8884	5.3324	5.6192	5.1690	7.9017
	0.049	2.9718	2.4442	3.2628	4.3432	7.0715
SCSS	0.011	5.7404	7.9472	12.6839	23.3048	39.6739
	0.035	4.8884	5.4206	5.2280	7.0062	7.3779
	0.049	2.9718	2.3531	3.4063	4.3358	7.3401
SCSC	0.011	7.6913	10.2019	14.7131	23.4962	39.6748
	0.035	5.1476	5.5688	4.5959	7.0230	7.3801
	0.049	2.3072	3.0312	2.9343	4.3478	7.3423

of the buckling coefficients predicted by two theories decreases as loading parameter increases which is more obvious for $\eta = 1.5, 2$.

5.2.2. *Effect of loading ratio on the buckling coefficient*

Figs. 23 and 24 display the variations of the buckling coefficient versus the loading parameter for SSSS and CCCC square plates when $h/a = 0.011, 0.035$ and 0.049 for IT and DT theories. It can be seen that for $h/a = 0.011$ a good agreement occurs between IT and DT results for various loading parameters for SSSS square plate, Fig. 23(a). Moreover, with increasing the thickness to length ratio, the discrepancy between IT and DT increases as the loading parameter increases, Figs. 23(b), 23(c), 24(b) and 24(c).

With increasing the linear loading parameter, the discrepancy between the results of two theories of plasticity increases. When the thickness of CCCC plate increases, $h/a \geqslant 0.035$, no agreements between the obtained buckling coefficients in various loading parameters are observed, Figs. 24(b) and 24(c). The discrepancy be-

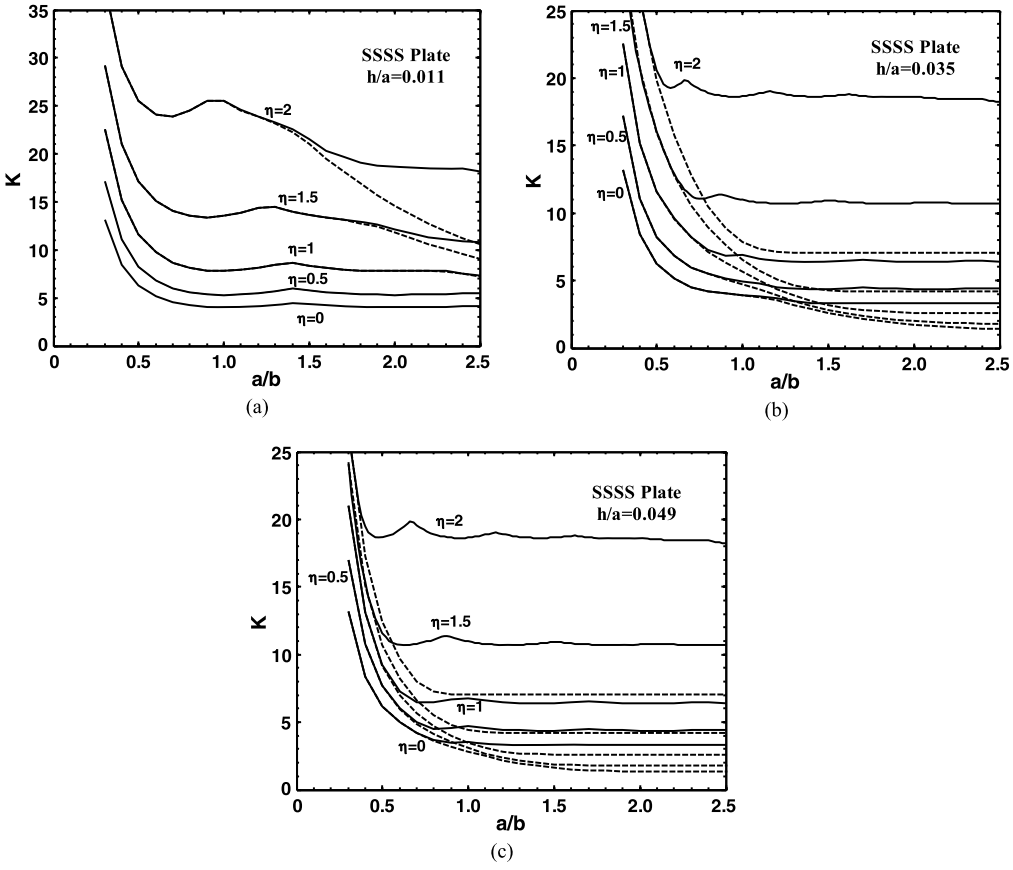

Fig. 20. Variations of buckling coefficient with aspect and thickness to length ratios for a linearly varying in-plane loaded SSSS plates under IT (solid line) and DT (dash line) predictions.

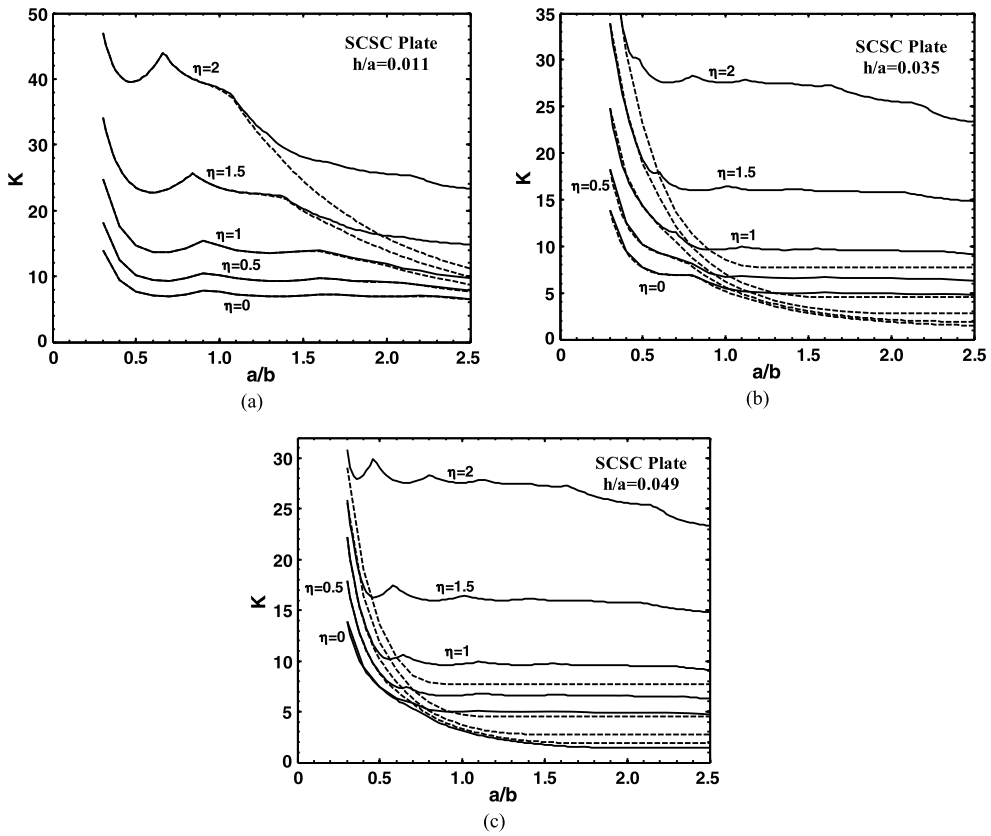

Fig. 21. Variations of buckling coefficient with aspect and thickness to length ratios for a linearly varying in-plane loaded SCSC plates under IT (solid line) and DT (dash line) predictions.

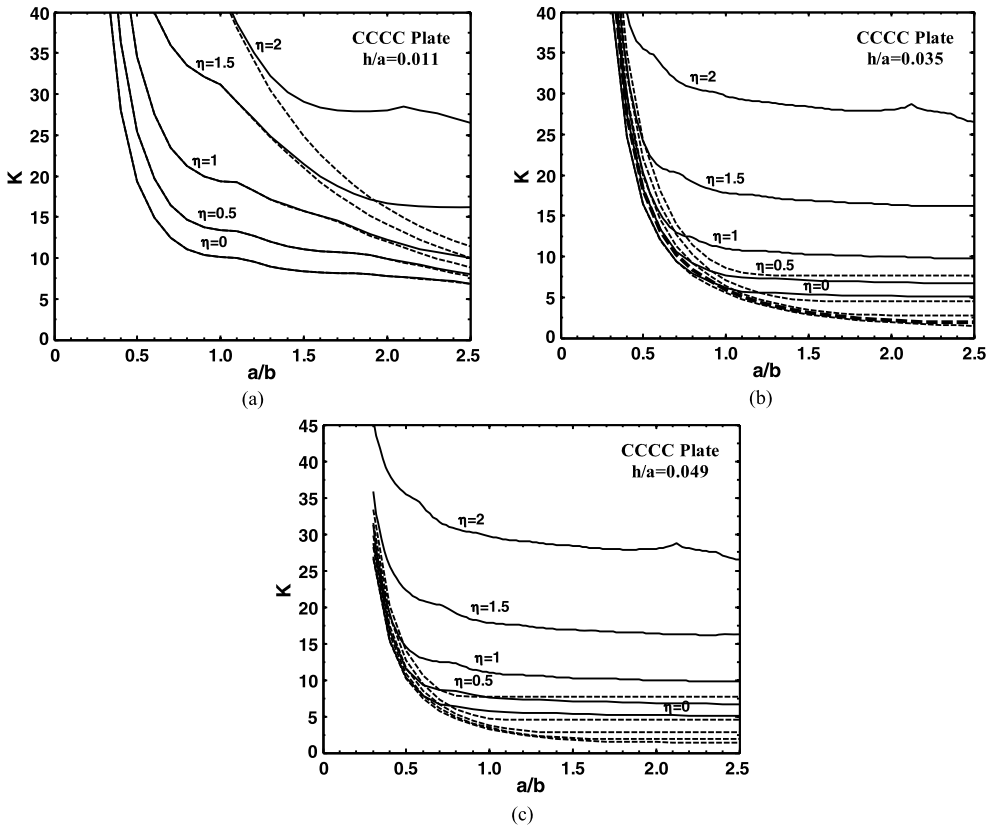

Fig. 22. Variations of buckling coefficient with aspect and thickness to length ratios for a linearly varying in-plane loaded CCCC plates under IT (solid line) and DT (dash line) predictions.

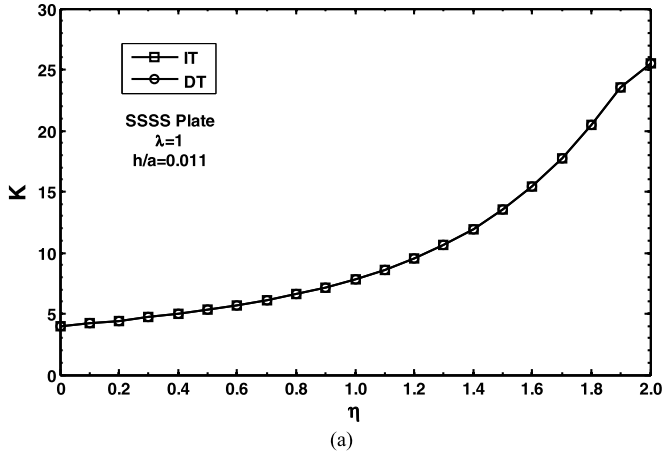

(a)

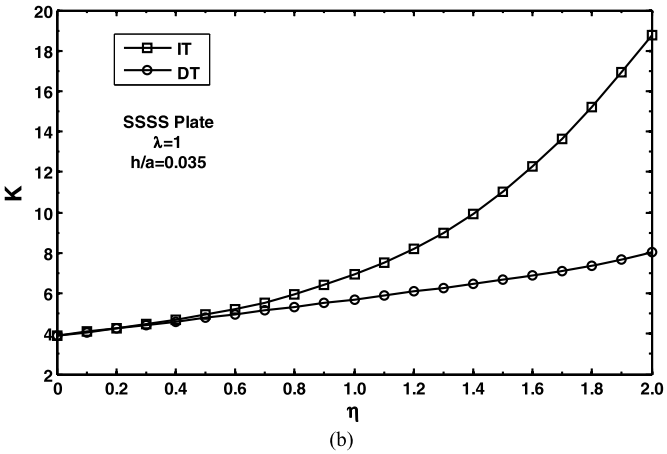

(b)

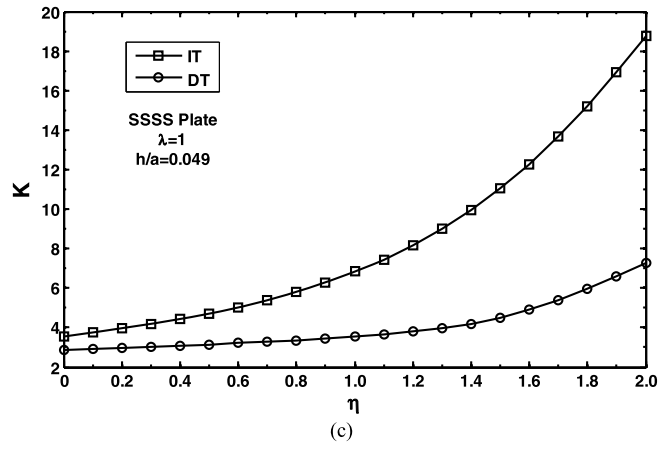

(c)

Fig. 23. Influence of loading factor on the buckling coefficient and thickness to length ratio for a linearly varying in-plane loaded SSSS square plates under IT and DT predictions.

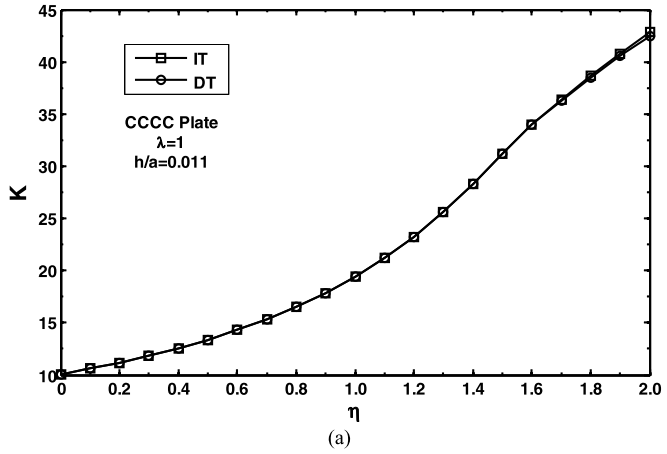

(a)

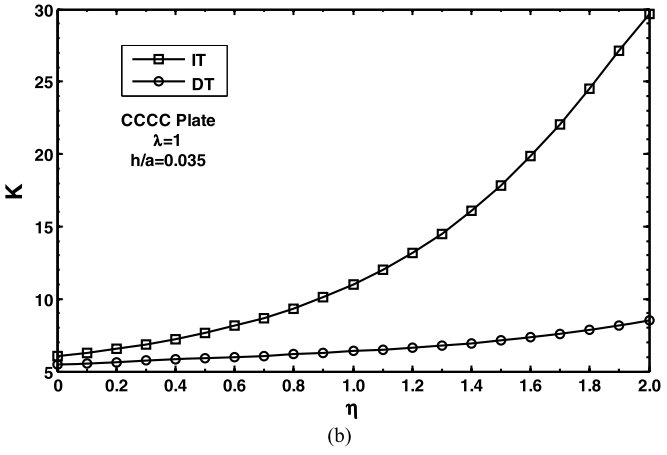

(b)

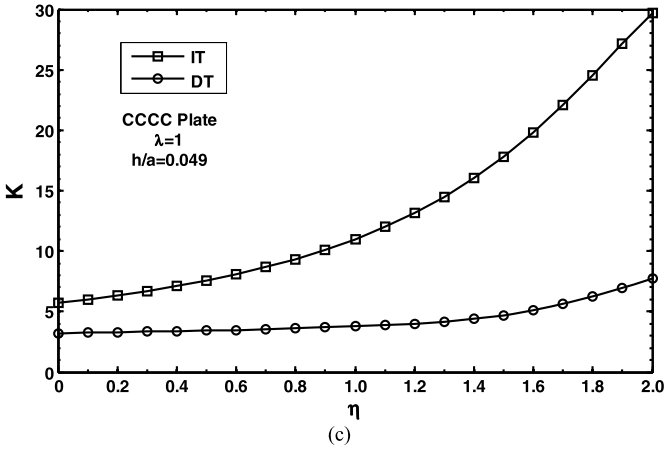

(c)

Fig. 24. Influence of loading factor on the buckling coefficient and thickness to length ratio for a linearly varying in-plane loaded CCCC square plates under IT and DT predictions.

tween IT and DT increases by applying the clamped boundary conditions and increasing thickness to length ratio, see Figs. 23 and 24.

5.2.3. Analysis of buckling mode shapes

In order to understand the buckling mechanism more accurately, the mode shapes of square plates for $h/a = 0.035$ are determined and depicted for SFSF, SSSS and CCCC boundary conditions by the aid of deformation theory of plasticity, Fig. 25.

The buckling mode shapes are affected by increasing of loading parameter significantly. As the loading parameter increases from 0 to 2, the bulges move toward the area of maximum compression of the plate, Fig. 25. For SSSS and CCCC plates, the buckling mode shapes in some cases have two or three longitudinal half-waves. One-half of the plate bulges out while the other half bulges in.

6. Conclusions

In the present paper, the equilibrium and stability equations for thin rectangular plate in plastic mode under various loadings were obtained. The constitutive equations were obtained based on IT and DT and the formulations and procedures were worked out in detail. The results were compared with previously published data to verify the established methodology and

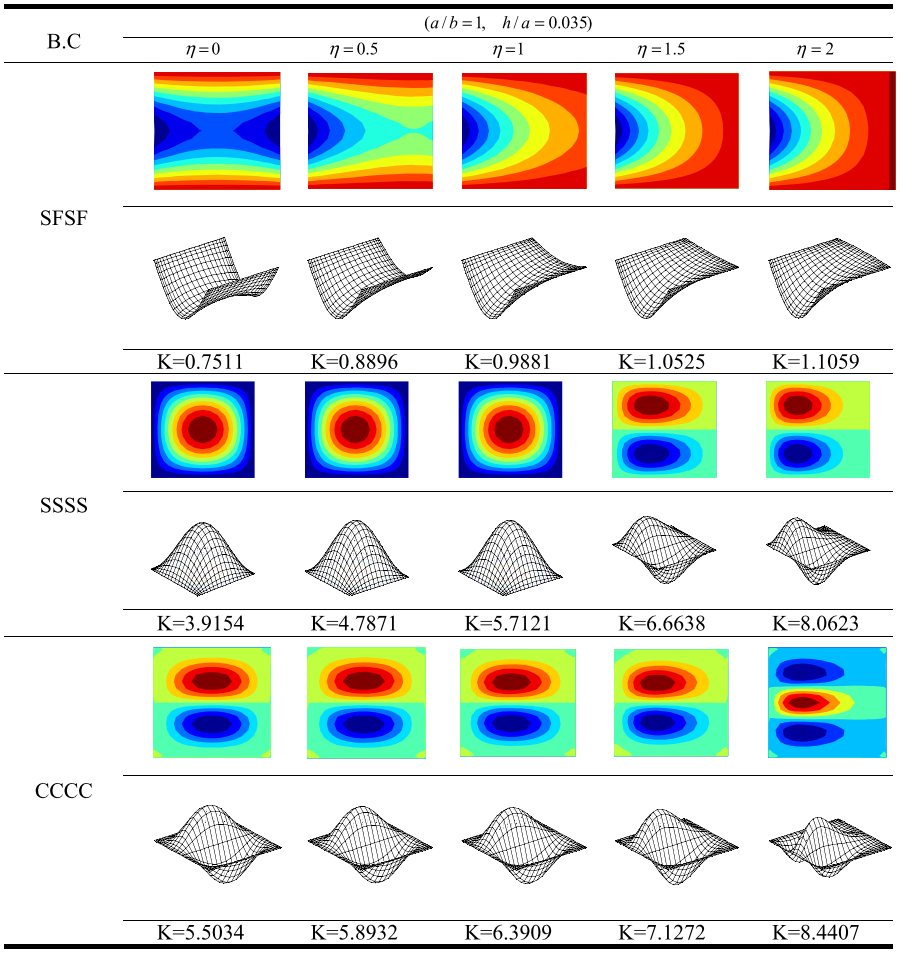

Fig. 25. Buckling mode shapes for SFSF, SSSS and CCCC square plates for various loading parameters.

procedures. The generalized differential quadrature method was used to solve the obtained equations. Unlike most previous studies, the various boundary conditions and linearly varying in-plane loading were considered in this study. The effects of aspect, thickness to length and loading ratios, boundary conditions, deformation and incremental theories and linearly varying in-plane loading on the buckling coefficient were studied in detail. Based on the numerical results, the following conclusions are reached:

- The aspect ratio has considerable effect on the buckling coefficient in IT especially for biaxial compression/tension loading.
- Plastic buckling coefficients depend on boundary conditions, thickness to length and aspect ratios, loading parameter and type of theory of plasticity.
- In biaxial compression/tension loading, unlike the uniaxial and equibiaxial loadings, with increasing the thickness to length ratio the results of the IT stand out of stress–strain curve gradually which shows this theory predicts invalid data.
- The variations of plastic buckling mode shape are less in equibiaxial compression rather than in uniaxial loadings. Moreover, the buckling mode shapes are more affected by loading parameter.
- The discrepancy between IT and DT increases by applying more clamped boundary conditions, increasing thickness to length ratio and using linear loading parameter.
- The buckling coefficient increases as the loading parameter changes from uniaxial compressive ($\eta = 0$) to pure in-plane bending ($\eta = 2$).
- In equibiaxial loading, the agreement between IT and DT results are more rather than uniaxial loading.
- With increasing the loading ratio in biaxial compression/tension, the differences between theories increase.

Appendix A

A.1. Incremental theory (IT) based on Prandtl–Reuss equation

This theory was first discussed by Prager (1938), Handelman et al. (1949), Hopkins (1949), Pearson (1950) and Besseling (1952) [13,18,6]. The constitutive equation in this theory is given by [9]:

$$E\dot{\varepsilon}_{ij} = (1+\nu)\dot{s}_{ij} + \left(\frac{1-2\nu}{3}\right)\dot{\sigma}_{kk}\delta_{ij} + \frac{3\dot{\sigma}}{2\sigma_e}\left(\frac{E}{T}-1\right)s_{ij}, \tag{A.1}$$

where s_{ij} is deviatoric stress tensor, T is tangential Young's modulus which is obtained from stress–strain curve and σ_e is the effective stress. The parameters T and σ_e are defined by

$$T = d\sigma_e/d\varepsilon_e, \qquad \sigma_e^2 = \sigma_x^2 - \sigma_x\sigma_y + \sigma_y^2 + 3\tau_{xy}^2. \tag{A.2}$$

A.2. Deformation theory (DT) based on Hencky equation

This theory was first discussed by Kollbrunner (1946), Ilyushin (1947), Stowell (1948), Bijlaard (1949) and Alghazaly (1986), [15,26,9,6]. The constitutive equation in this theory is given by [9]:

$$E\dot{\varepsilon}_{ij} = \left(\frac{3E}{2E_s} - \frac{1-2\nu}{2}\right)\dot{s}_{ij} + \frac{1-2\nu}{3}\delta_{ij}\dot{\sigma}_{kk} + \frac{3\dot{\sigma}}{2\sigma_e}\left(\frac{E}{T}-\frac{E}{S}\right)s_{ij}, \tag{A.3}$$

where S is secant Young's modulus determined by the uniaxial stress–strain curve.

References

[1] R.A. Anderson, M.S. Anderson, Correlation of crippling strength of plate structures with material properties, NACA Technical Note 3600, Washington, D.C., 1956.

[2] M. Aydin Komur, Elasto–plastic buckling analysis for perforated steel plates subject to uniform compression, Mechanics Research Communications 38 (2011) 117–122.

[3] R.E. Bellman, J. Casti, Differential quadrature and long-term integration, Journal of Mathematical Analysis and Applications 34 (1971) 235–238.

[4] J.P. Benthem, On the buckling of bars and plates in the plastic range, part II, NACA Technical Note No. 1392, Washington, D.C., 1958.

[5] C.W. Bert, M. Malik, Differential quadrature in computational mechanics: A review, Applied Mechanics Review 49 (1996) 1–27.

[6] J. Betten, C.H. Shin, Elastic–plastic buckling analysis of rectangular plates subjected to biaxial loads, Forschung im Ingenieurwesen 65 (2000) 273–278.

[7] J. Chakrabarty, Applied Plasticity, second ed., Springer, 2010.

[8] D. Durban, Plastic buckling of plates and shells, AIAA Paper 97-1245, NASA/CP 206280, 1998, pp. 293–310.

[9] D. Durban, Z. Zuckerman, Elastic/plastic buckling of rectangular plates in biaxial compression/tension, International Journal of Mechanical Sciences 41 (1999) 751–765.

[10] Kh.M. El-Sawy, A.S. Nazmy, M.I. Martini, Elastoplastic buckling of perforated plates under uniaxial compression, Thin-Walled Structures 42 (2004) 1083–1101.

[11] B. Geier, G. Singh, Some simple solutions for buckling loads of thin and moderately thick cylindrical shells and panels made of laminated composite material, Aerospace Science and Technology 1 (1997) 47–63.

[12] P.L. Grognec, A.L. Van, Some new analytical results for plastic buckling and initial post-buckling of plates and cylinders under uniform compression, Thin-Walled Structures 47 (2009) 879–889.

[13] G.H. Handelman, W. Prager, Plastic buckling of rectangular plates under edge thrusts, NACA Technical Note No. 1530, Washington, D.C., 1948.

[14] Sh. Hosseini-Hashemi, K. Khorshidi, M. Amabili, Exact solution for linear buckling of rectangular Mindlin plates, Journal of Sound and Vibration 315 (2008) 318–342.

[15] A.A. Ilyushin, The elastic plastic stability of plates, NACA Technical Memorandum, No. 1188, Washington, D.C., 1946.

[16] A.W. Leissa, J.H. Kang, Exact solutions for vibration and buckling of an SS-C-SS-C rectangular plate loaded by linearly varying in-plane stresses, International Journal of Mechanical Sciences 44 (2002) 1925–1945.

[17] T. Mizusawa, Buckling of rectangular Mindlin plates with tapered thickness by the spline strip method, International Journal of Solids and Structures 30 (12) (1993) 1663–1677.

[18] R.A. Pride, G.J. Heimerl, Plastic buckling of simply supported compressed plates, NACA Technical Note, No. 1817, Washington, D.C., 1949.

[19] G.H. Rahimi, M. Zandi, S.F. Rasouli, Analysis of the effect of stiffener profile on buckling strength in composite isogrid stiffened shell under axial loading, Aerospace Science and Technology 24 (2013) 198–203.

[20] C. Robert, A. Delameziere, P. Dal Santo, J.L. Batoz, Comparison between incremental deformation theory and flow rule to simulate sheet-metal forming processes, Journal of Materials Processing Technology 212 (2012) 1123–1131.

[21] E. Ruocco, V. Mallardo, Buckling analysis of Levy-type orthotropic stiffened plate and shell based on different strain-displacement models, International Journal of Non-Linear Mechanics 50 (2013) 40–47.

[22] S.C. Shrivastava, Inelastic buckling of plates including shear effects, International Journal of Solids and Structures 15 (1979) 567–575.

[23] C. Shu, Differential Quadrature and Its Application in Engineering, Springer, London, 2000.

[24] C. Shu, W. Chen, H. Xue, H. Du, Numerical study of grid distribution effect on accuracy of DQ analysis of beams and plates by error estimation of derivative approximation, International Journal for Numerical Methods in Engineering 51 (2001) 159–179.

[25] S.T. Smith, M.A. Bradford, D.J. Oehlers, Inelastic buckling of rectangular steel plates using a Rayleigh–Ritz method, International Journal of Structural Stability and Dynamics 3 (4) (2003) 503–521.

[26] E.Z. Stowell, A unified theory of plastic buckling of columns and plates, NACA Technical Note, No. 1556, Washington, D.C., 1948.

[27] S.P. Timoshenko, J.M. Gere, Theory of Elastic Stability, McGraw-Hill, New York, 1961.

[28] P. Tugcu, Effect of axial loading on plastic buckling of long strip under pure shear, International Journal of Computers and Structures 66 (1996) 155–161.

[29] C.M. Wang, T.M. Aung, Plastic buckling analysis of thick plates using p-Ritz method, International Journal of Solids and Structures 44 (2007) 6239–6255.

[30] X.W. Wang, J.C. Huang, Elastoplastic buckling analyses of rectangular plates under biaxial loadings by the differential quadrature method, Thin-Walled Structures 47 (2009) 14–20.

[31] C.M. Wang, Y. Xiang, J. Chakrabarty, Elastic/plastic buckling of thick plates, International Journal of Solids and Structures 38 (2001) 8617–8640.

[32] C.M. Wang, Y. Xiang, C.Y. Wang, Buckling and vibration of plates with an internal line-hinge via Ritz method, in: Proceedings of the First Asian-Pacific Congress on Computational Mechanics, Sydney, 2001, pp. 1663–1672.

[33] P. Weißgraeber, C. Mittelstedt, W. Becker, Buckling of composite panels: A criterion for optimum stiffener design, Aerospace Science and Technology 16 (2012) 10–18.

[34] W. Zhang, X.W. Wang, Elastoplastic buckling analysis of thick rectangular plates by using the differential quadrature method, Computers and Mathematics with Applications 61 (2011) 44–61.

[35] Z. Zong, Y. Zhang, Advanced Differential Quadrature Methods, Chapman & Hall /CRC, 2009.